Full length article

Shake table test and numerical analyses of a thin-walled Cold-Formed Steel structure: Part 1 — Investigation of the structural skeleton without claddings

George Taranu [a],*, Viorel Ungureanu [b], Zsolt Nagy [c], Mihai-Sergiu Alexa-Stratulat [a], Ionut-Ovidiu Toma [a], Septimiu-George Luca [a]

[a] The "Gheorghe Asachi" Technical University of Iasi, Faculty of Civil Engineering and Building Services, Department of Structural Mechanics, 700050, D. Mangeron no. 1, Iasi, Romania
[b] Politehnica University of Timisoara, Department of Steel Structures and Structural Mechanics, 300224, Ioan Curea no. 1, Timisoara, Romania
[c] Technical University of Cluj-Napoca, Faculty of Civil Engineering, No. 28, Memorandumului Street, Cluj-Napoca, 400114, Romania

ABSTRACT

CFS structures are classified as structures with low ductility. Due to this, they are not recommended for medium to high seismic areas. The paper presents the results of a complex experimental program coupled with numerical investigations on the behavior of Cold Formed Steel (CFS) structures under seismic actions. The scaled-down model skeleton was made of DX51D+Z C-shaped $89 \times 41 \times 12 \times 1$ mm steel elements connected by 4.8×16 mm self-tapping screws (STS) and 5.5×25 mm self-drilling screws (SDS). This structure represents a replica of constructive solutions for single-story or one or two-storey structures that are frequently met in South-Eastern Europe, including highly active seismic areas.

The main purpose of the research program is to gather both quantitative and, more importantly, accurate information regarding structural response to dynamic actions characterized by input accelerations equal in amplitude to the maximum values specified in seismic design codes, up to PGA = 0.40 g. The damage of the joints and the reduction in the structural stiffness due to cyclic loads, such as the ones produced by earthquakes, change the structure's eigen period and significantly influence the structure's response to seismic actions. Larger gravitational loads lead to more extensive damage of the joints. The developed numerical model based on the experimentally determined connection axial rigidity can offer accurate results in terms of the fundamental frequency of vibration, relative accelerations and displacements. However, for a more accurate capturing of the local damages and onset of failure mechanisms, more complex numerical models are needed, which take into account non-linear material behavior.

The results presented in this paper help to design these structures as only the skeleton and serve as a starting point for future research work aimed to assess the influence of the sheathing on the global response of CFS structures to seismic actions. Additionally, research in the direction of improved joints with better energy dissipation properties is also pursued by the authors.

1. Introduction

The behavior of civil engineering structures to seismic motions is a continuous matter of investigation for researchers around the world. Besides ensuring the safety of the inhabitants and mitigating the damages to the structures and the stored goods in the framework of performance-based design, buildings also need to become economic and sustainable in the sense that their maximum performance should be obtained with the least material consumption. Currently available seismic design codes, such as EN 1998-1 [1] or the Romanian code [2] include a lot of information and details on the seismic design of steel structures.

Based on their specifications, Thin-Walled Cold-Formed Steel Structures (TWCFSS) are classified as having low dissipative capabilities and the verification of structural elements included in Class 4 is made in accordance with EN 1993-1-3 [3], and EN 1993-1-5 [4], respectively. The seismic design codes limit the behavior factor q to 1.5 in [1] and to 1 in [2] because such structural systems without cladding materials have low energy dissipation capabilities. The values of the behavior factor q and the associated ductility classification which are given in the design codes, characterize the balance between resistance and energy-dissipation capacity. "For the design of structures classified as

Fig. 1. Structural type systems: (a) frame system; (b) panel; (c) panel with strips diagonal; (d) panel with diagonals system.

Fig. 2. Real House structural systems — personal archive: (a) Romania, 2018, (b) Germany, 2018.

low-dissipative, no account is taken of any hysteretic energy dissipation and the behavior factor may not be taken, in general, as being greater than the value of 1.5 considered to account for overstrengths". "The behavior factor q is an approximation of the ratio of the seismic forces that the structure would experience if its response was completely elastic with 5% viscous damping, to the seismic forces that may be used in the design, with a conventional elastic analysis model, still ensuring a satisfactory response of the structure" [1]. In this study, the behavior factor was not used. Based on the presented results future numerical analyses will be developed in order to determine the appropriate value of the behavior factor for such types of structures.

The seismic behavior of hot-rolled steel structures was the main subject of research until 1990. Several approaches were considered from scaled-down models to structural sub-systems, to individual structural elements. A very powerful equipment used in such experimental investigations, both for hot-rolled and cold-formed steel structures, is the shake table. It is the only equipment that can simulate real seismic motions of either past earthquakes or artificially generated ones. However, due to its high initial and maintenance costs, most experimental works included pseudo-dynamic tests on structural elements or parts of structures that can lead to obtaining similar results. Another alternative would be the use of numerical simulations where various parameters could be changed and many different scenarios could be considered. However, these numerical models should be validated by laboratory tests in order to ensure the accuracy of the obtained results [5,6].

Thin-walled cold-formed steel structures elements started to attract more and more attention from 1990 because of their gradual implementation in civil engineering structures. Their use has seen a continuous grow and a significant number of studies were published in USA [7–13], Italy [14–22], Romania [23–28], Turkey [29], UK [30,31] or Asia [32–43]. Each study considered different CFS profiles, structural system of connectors for joining the elements. The most used structural typologies consisted in 3D frames with built-up cross-sections for the elements or framing elements to form rigid systems for structural applications. Fig. 1 presents 4 of the main CFS structural systems that are currently in use. The solution presented in Fig. 1a is that of a portal frame using built-up cross-sections for the elements. The elements are connected at the nodes by means of hot-rolled steel plates and bolts. These are the so-called moment-resisting frames where the seismic force is dissipated due to the moment–rotation capacity of the joint. On the other hand, in case of framing systems made of shear wall panels, Fig. 1b, sheathing with either Oriented Strand Boards — OSB panels or corrugated steel sheets, the seismic force is dissipated by the panels/sheets and the connectors used to fix the panels onto the steel framing.

In the case of framing systems with vertical studs and diagonal steel strips, as shown in Fig. 1c, the seismic force is resisted by the framing and the diagonal elements. On the other hand, the truss-like framing system with rigid diagonal elements, Fig. 1d, is able to dissipate the seismic energy mainly through the diagonal elements. In either of the presented structural systems, the presence of OSB, corrugated steel sheet or any other sheathing panels greatly contribute to the dissipation mechanism of the seismic force. The efficiency of a scaled down two storey model, using the same structural approach presented in Fig. 1c, to seismic motion was demonstrated in a series of shake table tests conducted in 2009 at the "Gheorghe Asachi" Technical University of Iasi [44]. Additional experimental investigations on different structural typologies were conducted from 2016 to the present day [7,8,20,37, 45]. Such research works contribute to the general knowledge on the seismic behavior of steel structural systems and can be used to calibrate numerical models in order to conduct complex parametric investigations.

The structural model used in the present research is based on a framing concept with truss-like diagonal elements located in the marginal panels, as shown in Fig. 1d. Such system is frequently met in practice all over Europe, including in highly seismic active areas. Fig. 2 presents two examples of such structures built in Romania (see Fig. 2a), and Germany (see Fig. 2b), in 2018.

Fig. 3 presents an overview of a ground-floor building made from a combination of thin-walled cold-formed steel lipped channel profiles having the dimensions $89 \times 41 \times 12 \times 1$ mm and plain channel profiles with dimensions of $358 \times 78 \times 4$ mm.
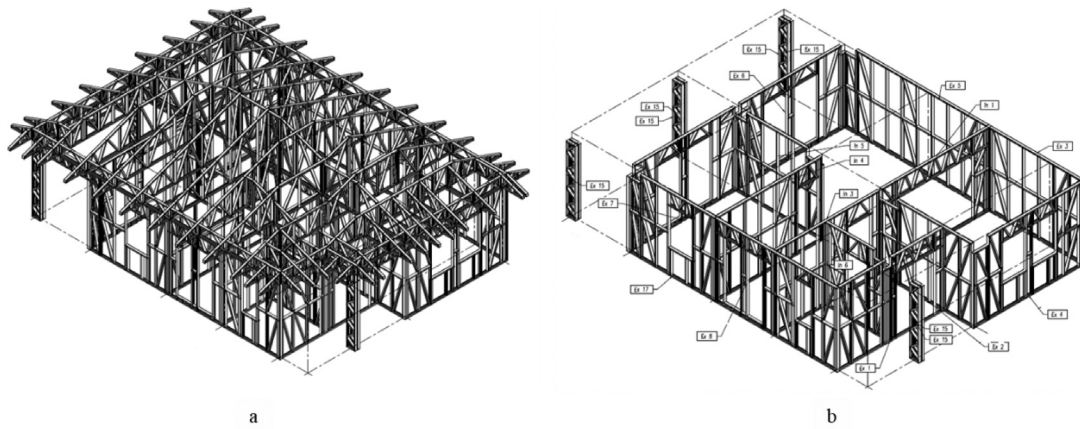
Fig. 3. Axonometry of typical one storey structural systems made of TWS profiles C89x41x12x1: (a) general assembly; (b) wall panel system.
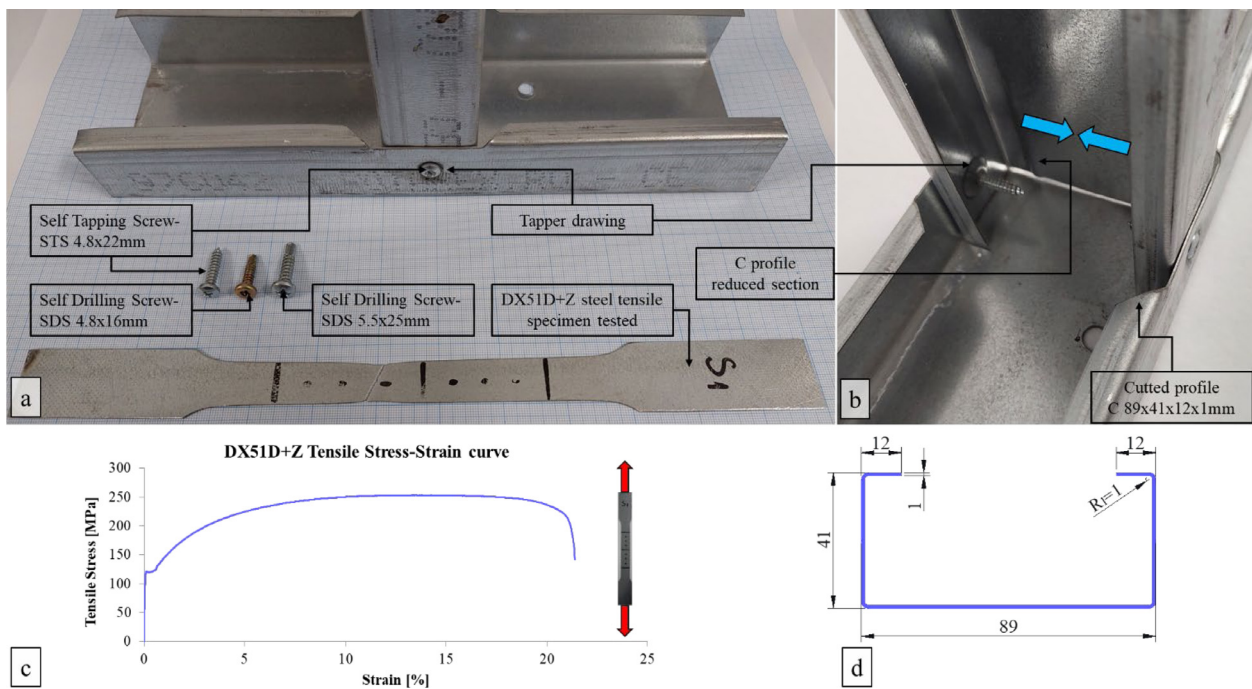
Fig. 4. (a) Materials and typical *T* joint connection; (b) perspective view of the connection with the interior; (c) average experimental tensile stress–strain curve of DX51D+Z steel sheet; (d) C profile section dimensions.

The lipped channels of 89 × 40×12 × 1 mm represents a relatively advantageous solution both for the end-user (beneficiary) and building-contractor due to its small overall dimensions. However, their use in structural elements to resist seismic loads should be considered only after significant experimental work in the laboratory. Such work could offer insightful information that can be used in the design practice. The obtained results are important data to calibrate numerical models based on FEM.

The present paper presents the results obtained from laboratory investigation on the material properties, behavior of T-joints to static and cycling loading scenarios and shake table tests to assess the be-havior of the structural system made of CFS frames with truss-like diagonal elements in the central panels. The experimental program is accompanied by numerical simulations in order to create a computer model that is able to simulate, as accurately as possible, the real behavior of the scaled-down model to seismic actions. Both linear and non-linear analyses were conducted to render evident the differences between the two approaches.

2. Materials and methodology

2.1. Structural materials and connectors

The material properties of the steel sheet and connectors are pre-sented in Table 1. The steel sheet used to obtain the steel profiles by cold-forming was DX51D+Z. Self-Tapping Screws (STS) with dimen-sions of 4.8 × 22 mm were used to connect the elements of the framing whereas Self Drilling Screws (SDS) with dimensions of 5.5 × 25 mm were used to connect the shear walls to each other. Additionally, the diagonal elements were connected by means of 4.8 × 16 mm SDS. The material properties of the steel sheet were experimentally determined by means of direct tensile tests on specimens cut from the profile web [46]. The material properties of the STS and SDS were the ones given by the manufacturer. The average stress–strain curve for the DX51D+Z steel is presented in Fig. 4a and the dimensions of the C-shaped profile are shown in Fig. 4b.

Table 1
Materials properties.

Element	Type	Elastic modulus (GPa)	Tensile yield strength (MPa)	Tensile ultimate strength (MPa)
Steel sheet C profiles — Fig. 4(a)	DX51D+Z	210	120 (exp)	250 (exp)
SDS — Fig. 4 (a) for profile connections ISO 15481 class (5.6) [47]	4.8 × 16 mm	210	300 [48]	500 [48]
SDS — Fig. 4 (a) for panel connections ISO 15481 class (5.6) [47]	5.5 × 25 mm	210	300 [48]	500 [48]
STS — Fig. 4 (a) for profile connections ISO 7049 class (5.6) [49]	4.8 × 22 mm	210	300 [48]	500 [48]
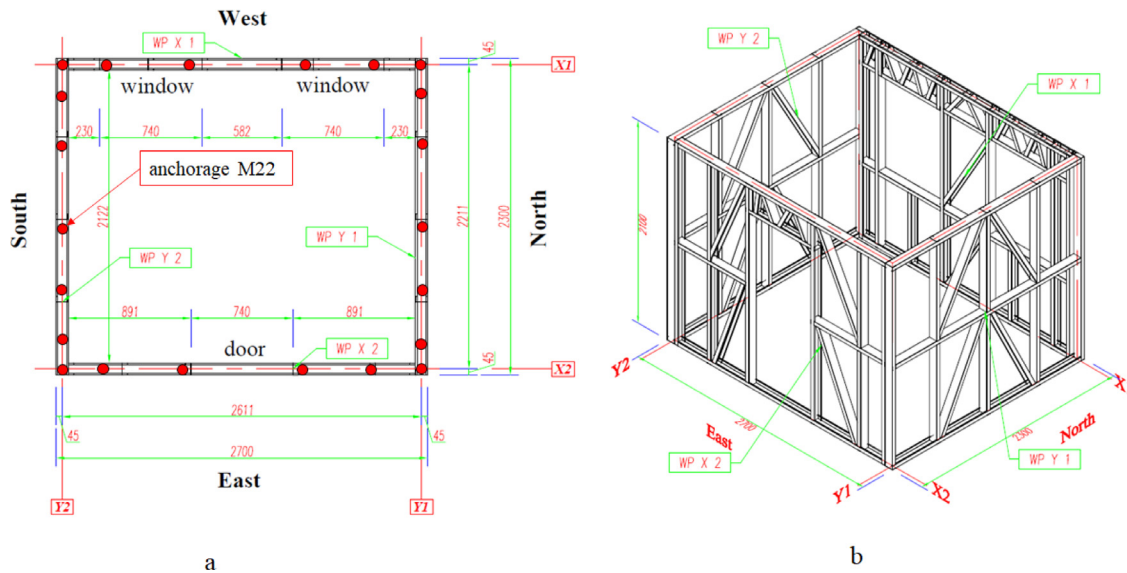
Fig. 5. (a) Plan view of the structural model; (b) Axonometry of the wall panels.
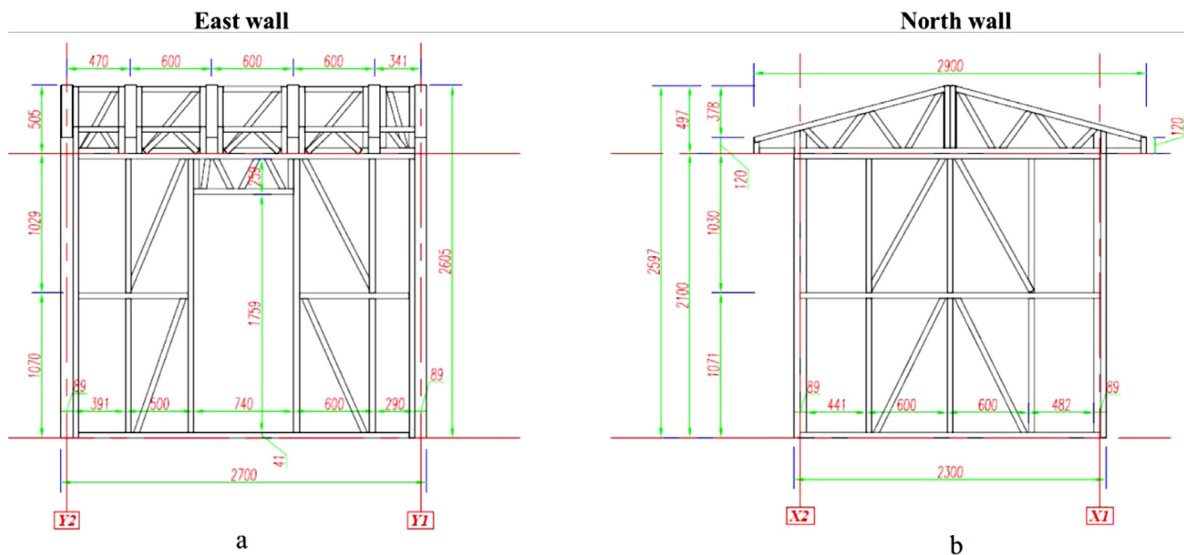
Fig. 6. Front views of the walls: (a) East wall, X1 direction; (b) North wall, Y1 direction.

2.2. Structural model assembly

The scaled-down model, presented in Fig. 5, had the in-plane dimensions of 2700 × 2300 mm, wall height of 2100 mm and the total height (at the ridge) of 2597 mm. The model was made of four panels. The roof was made of trusses with inclined upper chords, as shown in Fig. 6, transversally positioned (Y direction in Fig. 5). The stiffness of the roof was ensured by using truss panels located on top of the

longitudinal wall panels (X direction in Fig. 5) and at the middle of transversal wall panels. The longitudinal wall panels had openings for windows and doors.

Fig. 5a presents the in-plane view of the model whereas Fig. 5b presents the axonometric view of the wall panels. The North–South direction of the model coincides with the X axis of the shake table along which the shaking motions will be induced. The East wall has a door opening with the dimensions of 740 × 1759 mm and the opposite, West,

Table 2
Similarity relationship and Cauchy similitude scaling factors.

Parameter	Symbol	Prototype	Model	Scale factor (prototype/ model)	Scale factor value
Length	L	3240 (mm)	2700 (mm)		
Width	w	2760 (mm)	2300 (mm)	$L_p/L_m = \lambda$	1.2
Height	h	3126 (mm)	2605 (mm)		
Steel profile section	sps	C 89 × 40 × 12 × 1 (mm)	C 89 × 40x12 × 1 (mm)	$L_p/L_m = \lambda$	1
Elasticity modulus	E	210000 (N/mm^2)	210000 (N/mm^2)	$e = E_p/E_m$	1
Specific mass	ρ	7850 (kg/m^3)	7850 (kg/m^3)	$\rho = \rho_p/\rho_m$	1
Mass	m	506 (kg)	293 (kg)	$m = m_p/m_m = \lambda^3$	1.728
Displacement	d			$d = d_p/d_m = \lambda$	1.2
Velocity	v			$v = v_p/v_m$	1
Acceleration	a			$a_p/a_m = 1/\lambda$	0.833
Time	t			$t_p/t_m = \lambda$	1.2
Frequency	f			$f_p/f_m = \frac{1}{\lambda}$	0.833

Fig. 7. Connection details: (a) panel intersection connection; (b) current joint of diagonals; (c) upper part T joint connection; (d) screws details; (e) base fixing detail.

wall had two window openings with dimensions of 740 × 1000 mm. The X1 and X2 represent the axes of the longitudinal walls and Y1 and Y2 represent the axes of the transversal walls.

The geometrical dimensions of the East wall and North wall are presented in Fig. 6. North and South wall panels are identical to one another whereas East and West wall panels have different configuration to accommodate the door and window openings. The wall framing panels were obtained by connecting the CFS elements by means of 4.8 × 16 mm STS that fit in the drawings located at the theoretical longitudinal axes of the steel profiles. The model was fixed on the shake table by 14 M22 bolts (4 bolts in both X1 and X2 directions and 3 bolts on both Y1 and Y2 directions).

The scaling down of the model was bound by the dimensions of the ANCO R250 shake table. Table 2 summarizes the values of the scaling factor based on the Cauchy law of similarity [50,51].

The joining of the steel profiles presented drawings, the diagonal members and the struts had reduced cross-sectional height and the clipping of the C-profile flanges was performed for the contour elements. Details of the joint layouts are presented in Fig. 7.

2.3. Test set-up and data acquisition

The experimental program took place at the Department of Structural Mechanics from the "Gheorghe Asachi" Technical University of Iasi. The 3-DOFs ANCO R-250 shake table has the in-plane dimensions of 3000 × 3000 mm. The 600 kN electro-hydraulic actuators are located at 120 degrees, as shown in Fig. 8. The frequency range is between 0–30 Hz whereas the maximum acceleration can reach 3 g. The fixing on the models on the shake table can be done using M22 bolts in a grid having the 200 step-size in both in-plane directions.

The scaled-down model was fitted with 4 PT5 A displacement transducers denoted as $D_{x1} \ldots D_{x4}$ in Fig. 8. The shaking motion was applied in the X direction, as shown in Fig. 8. The response of the model, in terms of accelerations, was recorded by means of four DYTRAN 3202 A accelerometers (A_{x1}, A_{x2}, A_{y1} and A_{y2}) located at the eaves, as shown in Fig. 9. The sampling frequency of the ESAM traveler data acquisition system was set at 50 recordings/ second/ channel.
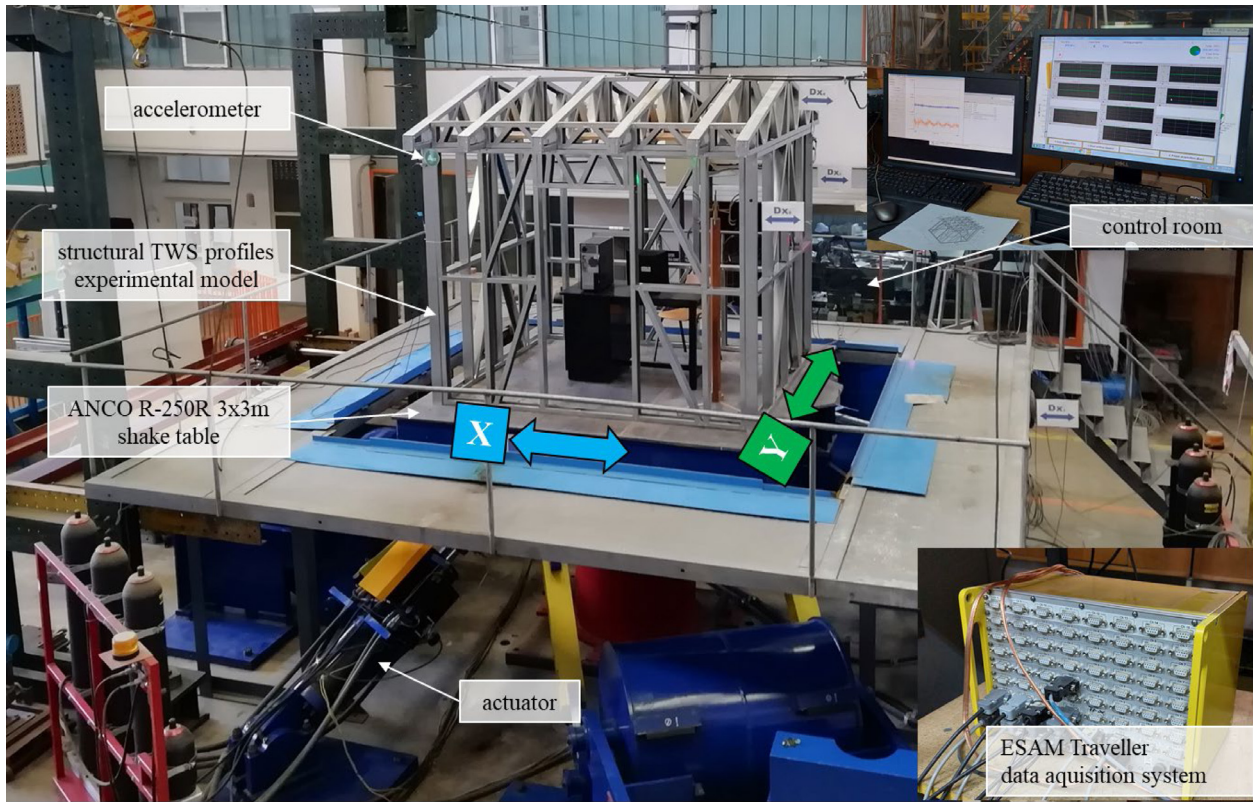
Fig. 8. View of the model on the shake table and instrumentation position.
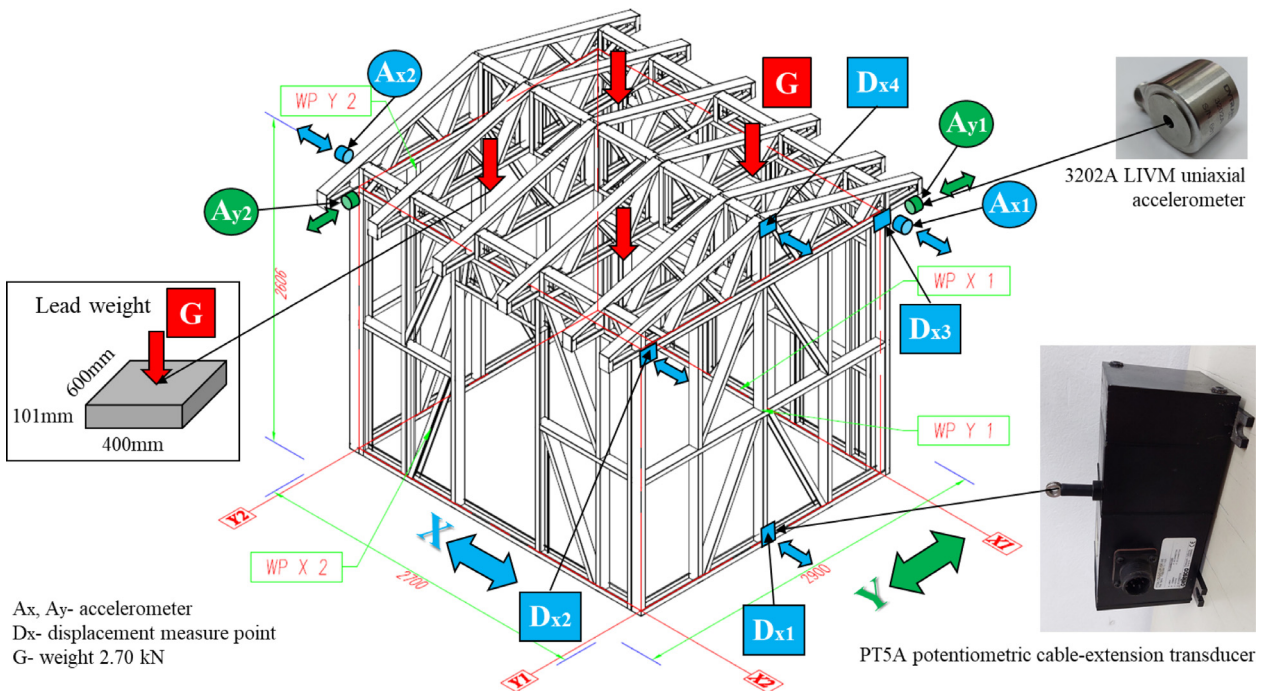
Fig. 9. Axonometry of the structural model with displacement LVDT positions.

3. Experimental program

3.1. Dynamic motions

According to the seismic design codes [1,2] and taking into account the seismic zoning of Romania, shown in Fig. 10, there are three distinct values for the corner/control period T_C: 0.7 s, 1.0 s and 1.5 s. The peak ground acceleration (PGA) in the Vrancea area, epicentral zone, is 0.4 g for a return period of 225 years and a 20% probability of being exceeded in 50 years. Sine beat loading function was chosen with 1 Hz, 1.5 Hz and 6 Hz frequencies and acceleration amplitudes between 0.14 g and 0.71 g.
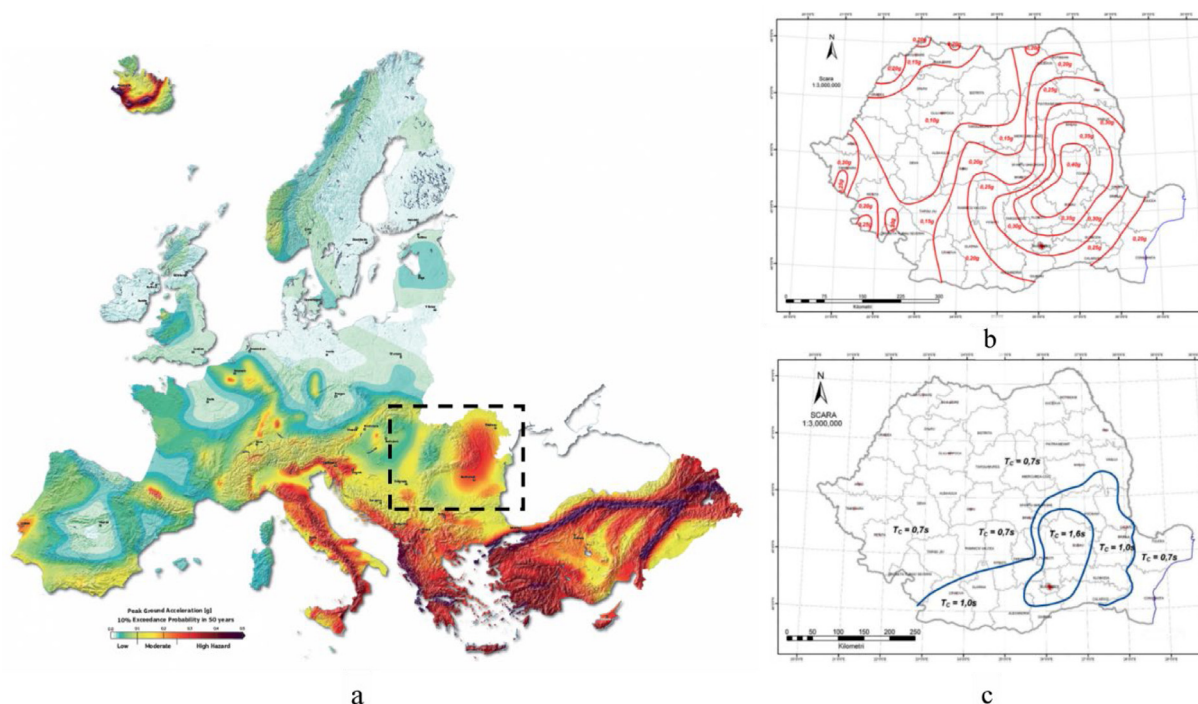
Fig. 10. (a) Europe seismic map [52]; (b) Romania — PGA for a RMI of 225 years and 20% probability of exceedance in 50 years; (c) Zonation of Romania based on the control/corner period T_C, of the response spectrum [2].

3.2. Loading scenarios

The experimental program considered two distinct cases in terms of live loads: bare frame without any additional gravitational loads (Unloaded-UL) and additional masses located at the top part of the walls. The additional masses, shown in Fig. 9, consisted of lead weights, each weighing 275 kg. They were symmetrically located at the ceiling level representing an equivalent load of 1.80 kN/m^2. The dynamic characteristics of the model were firstly determined after which shaking motions were induced following a sine-beat function with different frequencies and different amplitudes of accelerations.

The total load $q = q_1 + q_2 + q_3 + q_4 = 1.80$ kN/m^2 represented the contribution of permanent and partial snow loads considered with their most unfavorable intensities:

- Tile roof $q_1 = 0.75$ kN/m^2;
- Additional steel profiles for cladding: $q_2 = 0.12$ kN/m^2;
- Covering elements: $q_3 = 0.3$ kN/m^2;
- 40% of the snow load with $s = 2.5$ kN/m^2: $q_4 = 0.63$ kN/m^2;

Table 3 summarizes the loading protocol. The different frequencies of the sine-beat function as well as levels of accelerations would offer sufficient data to better understand the behavior of the CFS model to seismic actions.

There are two categories of tests presented in Table 3. The tests denoted with F are those for which the fundamental frequency of vibration was measured in the initial, undamaged state, and after each series of dynamic tests. The tests denoted with T are the test involving the dynamic sine-beat motions. The number in the test designation means the frequency of the shaking motion. Hence, F0-UL-1 Hz represents the test conducted to determine the fundamental frequency of vibration in the initial, unloaded (UL) state. Consequently, T10-L-1 represents test number 10, conducted on the loaded model (L) and the shaking motion had a frequency of 1 Hz.

3.3. Cyclic loading tests on T-joints

The shake table tests were preceded by cyclic loading tests on the T-joints with different configurations in terms of used connectors: type

A with 4.8×16 mm SDS, type B with 4.8×22 mm STS and Tapper drawing and type C using a combination of types A and B. A detailed presentation of the research work can be found in [46]. For the purpose of this study, only type B joints were considered.

In case of structures subjected to seismic motions, the behavior of joints to cycling loads is very important because it can give information related to the possible deformations and decrease of rigidity. The cyclic tests were conducted in accordance with the methodology outlined in [53,54]. Five T-joint specimens were considered. They were first subjected to 20, displacement controlled, cyclic tests with a maximum amplitude of $+/-1$ mm and a loading rate of 0.083 mm/s. After the 20 cycles, the amplitude was increased to $+/-2$ mm and the loading rate to 0.167 mm/s and an additional 20 cycling tests were performed. An electro-hydraulic Zwick/Roell 1000SP universal testing machine was used to run this part of the experimental program (see Fig. 11).

4. Experimental results

4.1. Results of cyclic tests on the T-joint

Fig. 12 presents the average load–displacement curves obtained during the cyclic tests. It can be observed that for a maximum displacement of $+/-1$ mm, Fig. 12a, the stiffness on the tensile part of the test is almost constant with a value of 2300 N/mm and did not decrease significantly after 20 loading cycles. The peak load corresponding to the maximum displacement of 1 mm was 2300 N la 1 mm. On the compression part of the curve however, two different behaviors could be observed: from 0 to -0.5 mm the average value of the stiffness was 2200 N/mm. From -0.5 mm to -1.0 mm the stiffness increased to 8896 N/mm. A more evident decrease in the value of the stiffness can be observed after 20 loading cycles, especially for displacements between -0.5 mm to -1.0 mm. The variation in the applied force amplitude with the number of loading cycles, both in the tensile and compression ranges of the load–displacement curve is presented in Fig. 12c. It can be observed that the intensity of the applied load in the tensile range is almost constant whereas a significant decrease could be seen in the compression range. The value of the secant stiffness,

Table 3
Experimental test.

Curre nt no.	Test label	Description	Dead load (kN/m^2)	Action type	Action frequency (Hz)	Action period (s)	Action max. abs. acceleration (g)	Percent of max. PGA seismic design code (0.4g)	Max. shake table abs. displacement in X direction (mm)
1	F0-UL-1Hz						-	-	-
2	T1-UL-1						0.21	52.5%	52.44
3	T2-UL-1				1	1	0.31	77.5%	73.34
4	T3-UL-1						0.43	107.5%	102.4
5	F1-UL-1Hz						-	-	-
6	T4-UL-1.5	Unloaded model (UL) tests		Sine beat			0.36	90%	39.88
7	T5-UL-1.5		0		1.5	0.667	0.51	127.5%	55.62
8	T6-UL-1.5						0.71	177.5%	76.85
9	F2-UL-1.5Hz						-	-	-
10	T7-UL-6						0.14	35%	1.26
11	T8-UL-6				6	0.167	0.23	57.5%	2.56
12	T9-UL-6						0.33	82.5%	3.87
13	F3-UL-6Hz						-	-	-
14	F4-L-1Hz						-	-	-
15	T10-L-1						0.22	55%	52.92
16	F5-L-1Hz	Loaded model (L) tests		Sine beat			-	-	-
17	T11-L-1 (FEM correlation)		1.80		1	1	0.31	77.5%	72.89
18	F6-L-1Hz						-	-	-
19	T12-L-1 (collapse)						0.46	115%	100.49
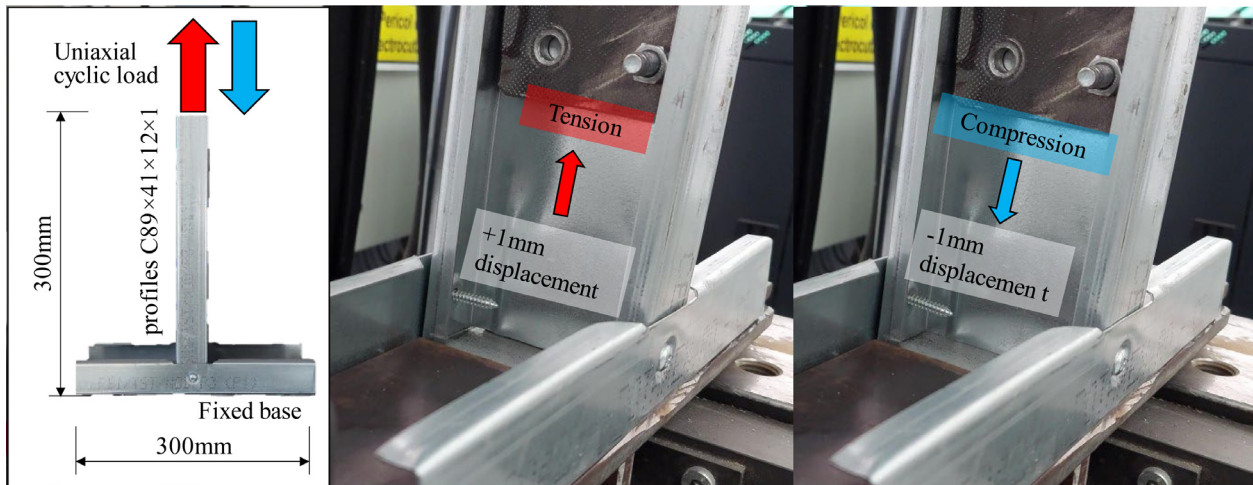
Fig. 11. Tension–Compression cyclic loading experimental test +/−1 mm @0.083 mm/s.

after 20 loading cycles, stabilized around de 2300 N/mm. After the initial test, a second round of cyclic tests were conducted on the same samples of T-joints with double the amplitude of the displacement: +/−2 mm. This resulted in a decrease in the values of the secant stiffness by approximately 30%, Fig. 12b, and almost constant intensity of the applied load both in tension and a smaller decrease of the load in compression, Fig. 12d.

4.2. Dynamic properties of the scaled down-model

The fundamental frequency of vibration for the unloaded, undamaged model was determined using the free-vibration decay method. The scaled-down model was then subjected to a first set of seismic motions at a motion frequency of 1 Hz (tests T1–T3 from Table 3). The fundamental frequency of vibration was then measured again at the end of the first series of tests. The experimental program continued with a second series of seismic motions with a motion frequency of 1.5 Hz. After a third determination of the fundamental frequency, the bare frame model was subjected to a third series of shake table test with a frequency of 6 Hz (tests T7–T9, Table 3). The change in the fundamental frequency of vibration from one series of tests to another, for the bare frame, is presented in Fig. 13a. The model was then loaded, as described in Section 3.2. The addition of masses changed the

fundamental frequency from 8.09 Hz to 2.98 Hz, a 278% decrease. For the loaded model only one test was conducted for the motion frequency of 1 Hz but with different amplitudes (tests T10–T12, Table 3). The change in the fundamental frequency for the loaded model is presented in Fig. 13b

Based on the obtained data it can be concluded that the model exhibited some slight damages which is reflected in a decrease of the fundamental frequency from 8.28 Hz to 8.09 Hz for the unloaded scenario, a 2.41% decrease compared to the initial stage. A more significant decrease in the value of the fundamental frequency could be observed when the model was loaded with additional masses, the change being 31.21%.

4.3. Response of the model in accelerations

Fig. 14 presents the input versus recorded accelerations at the level of the shake table and at the top part of the walls for the model as an average value of the records given by accelerometers A_{x1} and A_{x2} (see Fig. 9). It can be observed that for the first series of tests (input frequency 1 Hz and different values for the acceleration amplitudes) the model behaves rigidly, with very small values of the relative accelerations computed as the difference between the absolute accelerations at the top of the walls and the absolute accelerations recorded at the
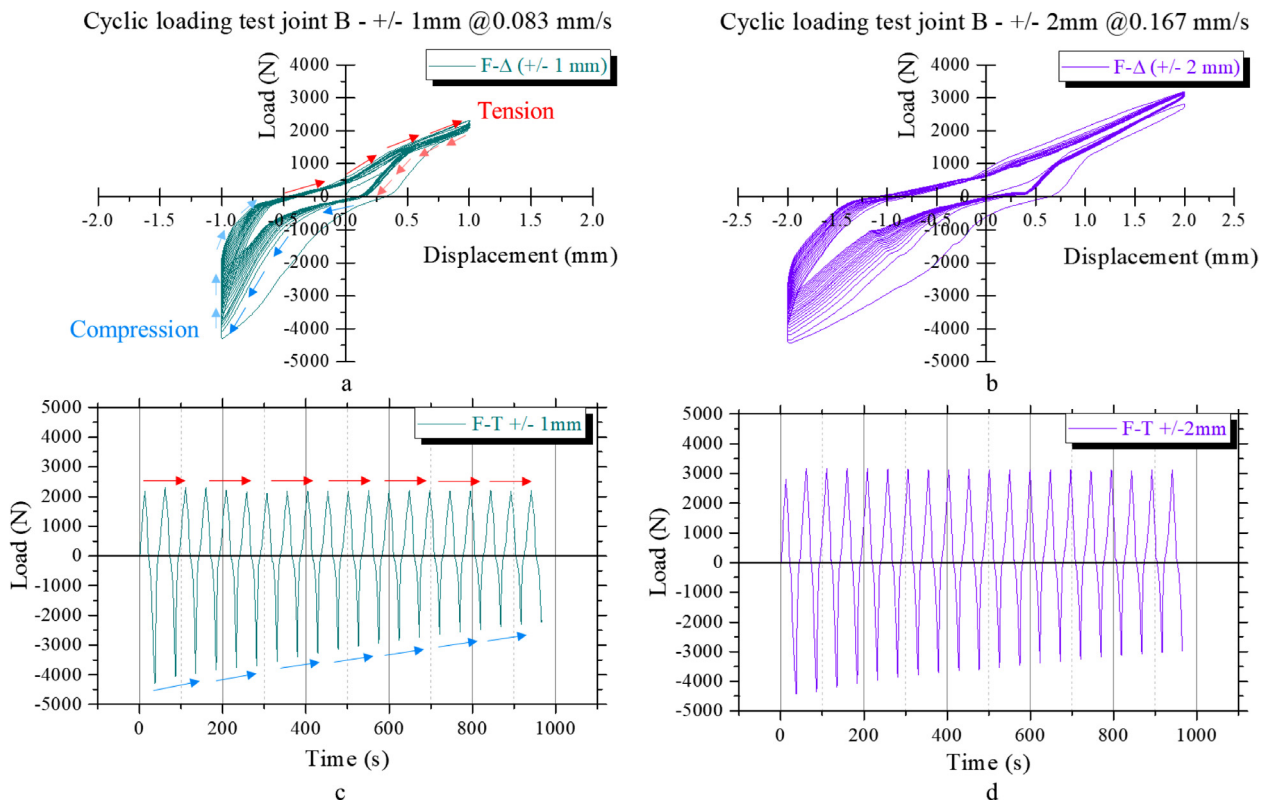
Fig. 12. Tension–Compression cyclic test results: (a) joint B +/−1 mm @0.083 mm/s; (b) joint B +/−2 mm @0.167 mm/s; (c) Load vs. time evolution of cyclic test with +/−1 mm; Load vs. time evolution of cyclic test with +/−2 mm.
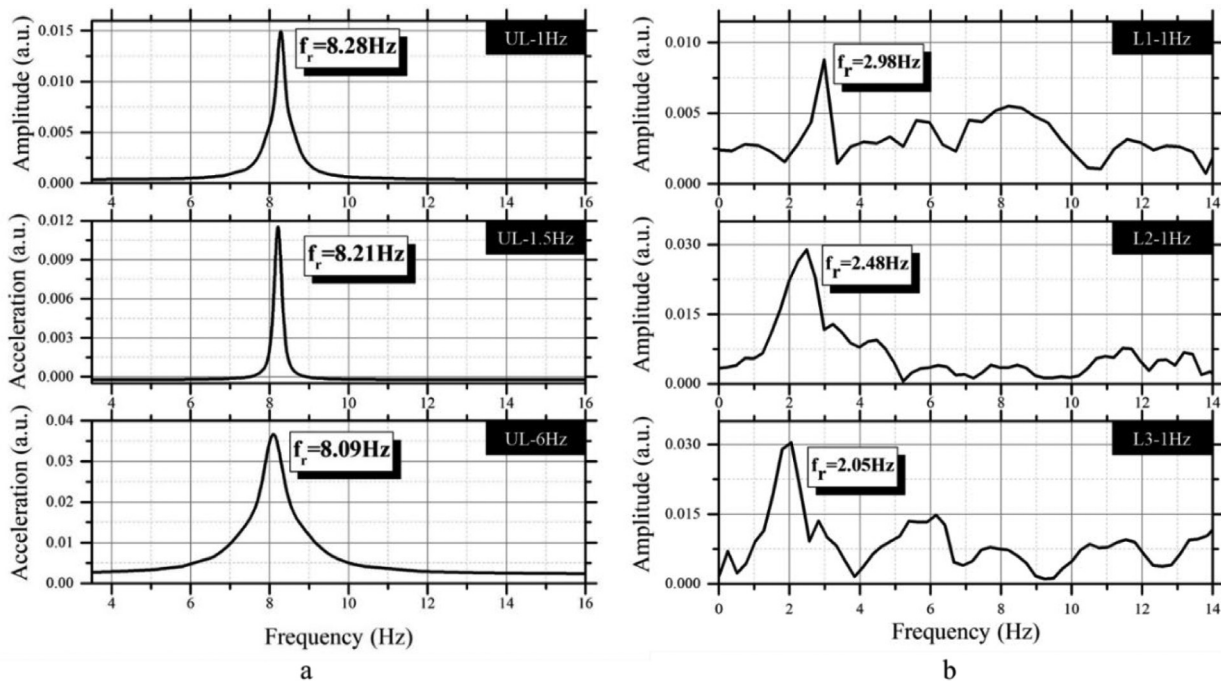
Fig. 13. Results of dynamic identification in terms of natural frequency (a) -Unloaded Model — UL; (b) Loaded Model — L..

level of the shake table. There is, however, an instance during test T3 when the maximum amplitude of the relative acceleration was 0.48 g.

Increasing the frequency of the input motion to 1.5 Hz did not result in significant change in the behavior of the model. It can be seen that the model and the shake table are in phase with one-another. The amplitude of the relative acceleration was reached a maximum of

0.34 g during test T5. From the data of the two series of tests it can be concluded that no significant amplifications were observed.

Increasing the frequency of the input motion to 6 Hz resulted in significant amplifications of the response. In test T9, even though the amplitude of the input motion was 0.33 g, the maximum relative acceleration was 1.76 g. This could be explained by the fact that the
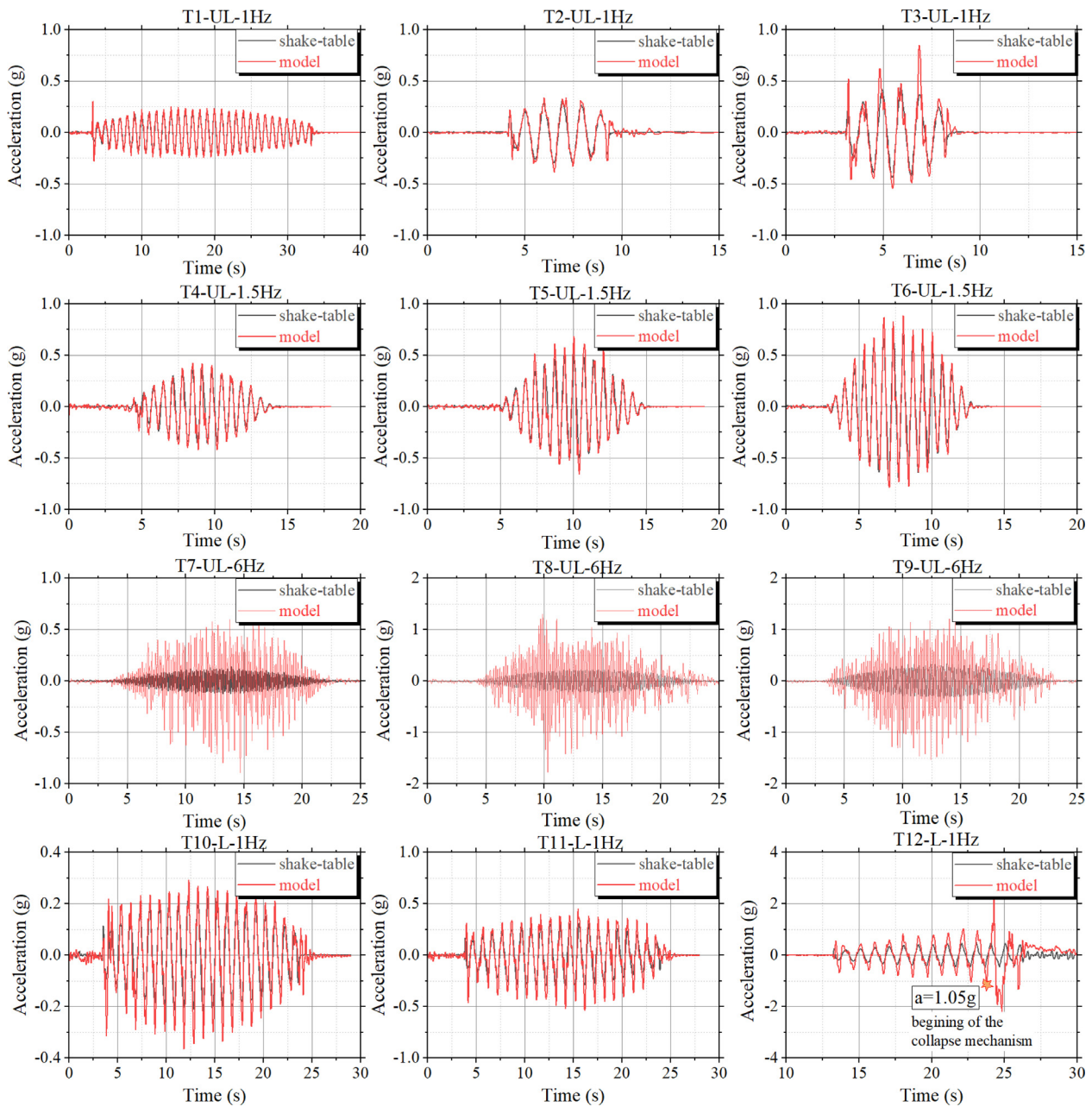
Fig. 14. Absolute acceleration vs. time of the experimental tests.

frequency of the input motion is closer to the fundamental frequency of vibration of the model and therefore significant amplifications of the response were observed.

When the model was loaded by additional masses, the amplitude of relative accelerations increased from 0.4 g in case of test T11 to 0.92 g in case of test T12 before the failure mechanisms started to develop. When the amplitude of the absolute acceleration of the model exceeded 1.05 g, the model failed, and the test was stopped. This can be seen from the last graph in Fig. 14 when the input and response motions are clearly out of phase and significant amplifications of the input amplitude were observed.

4.4. Relative lateral displacements

Fig. 15 presents the time histories of the relative lateral displacements computed as the difference between the average values measured by the displacement transducers D_{x2} and D_{x3} and the displacements recorded by D_{x1} (see Fig. 9).

The recorded data is consistent to what was presented in Fig. 14. Lower values of the relative lateral displacements were observed for the first two series of test with input frequencies of 1 Hz and 1.5 Hz, irrespective of the acceleration amplitudes. The maximum relative lateral displacement for the first series of tests was obtained for test T3, 2.99 mm, whereas for the second series the maximum relative displacement was 3.07 mm.

When the frequency of the input motion increased to 6 Hz, significant amplification of the response was observed during tests T8 and T9 for which the relative lateral displacements were 12.8 mm and 13.44 mm, respectively.

The loaded model exhibited significantly larger relative displacements from 22.75 mm for test T10 to 55.03 mm for test T12 before the failure mechanisms started to develop. A relative displacement of 283.14 mm was recorded when the collapse of the model occurred.

Table 4 summarizes the results in terms of fundamental frequencies of vibration as well as maximum amplitudes of relative accelerations and displacements.
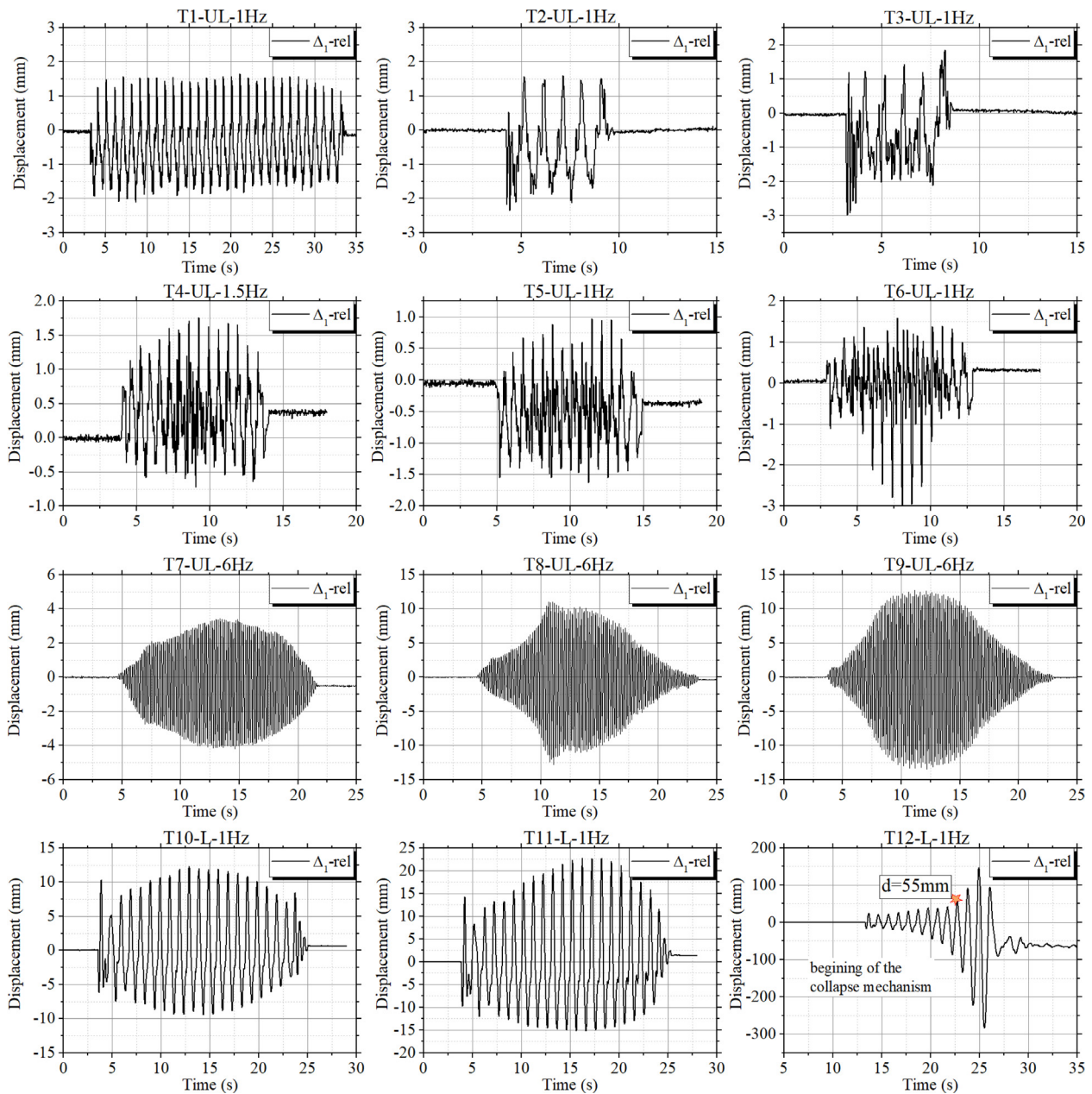
Fig. 15. Relative displacement vs. time: (a) Unloaded tests T3, T6, T9; (b) Loaded model tests T10, T11, T12.

4.5. Base shear–relative displacement curves

Fig. 16 presents the base shear–relative displacements curves for the tests of highest amplitude of the input motion in case of the bare frame model (T3, T6 and T9) as well as all three tests conducted on the loaded frame (tests T10–12).

According to the Romanian seismic design code, the maximum relative displacement in case of serviceability limit state (SLS) should be less than $0.005H$ where H is the height of the structure. For the model presented in this research work the maximum allowable displacement in case of SLS would be 10.5 mm.

$$d_r^{SLS} = 0.005H = 0.005 \cdot 2100 = 10.5 \text{ mm} \tag{1}$$

In case of ultimate limit state (ULS), the relative displacement should not exceed $d_r^{ULS} = 0.025H$, where H is the height of the structure. For the model presented in this research work the maximum allowable displacement in case of ULS is 52.5 mm.

$$d_r^{ULS} = 0.025H = 0.025 \cdot 2100 = 52.5 \text{ mm} \tag{2}$$

Analyzing the data presented in Fig. 16 it can be concluded that the scaled down model behaves linearly for the most part of the tests although in case of test T9 larger values were obtained for the relative lateral displacement which could mean that some of the joints exhibited larger deformations. For the loaded model, the relative displacement exceeds 20 mm in case of test T11 and a decrease in the overall stiffness can be observed. The values of the relative displacement become more significant during test T12, reaching 55.03 mm which represent the onset of the failure mechanisms.

4.6. Failure mechanisms

4.6.1. T-joints subjected to cyclic loading

The following failure mechanisms could be observed during the cyclic tests performed on the T-joints with 4.8 × 22 mm STS. Their order of development is presented in Fig. 17. Due to the cyclic loading the screw, which can be assumed as a small cantilever, tilts downwards due to the tensile force being applied, mechanism (a), almost at the

Table 4
Experimental test results.

Test no.	Test label	Natural frequency (Hz)	A_{TX} PGA abs shake table (g)	A_x abs. max structure (g)	A_x rel. max (g)	$\Delta_{1max} = D_{x3} - D_{x1}$ (mm)	$\Delta_{2max} = D_{x4} - D_{x1}$ (mm)
1	F0-UL-1Hz – F.D.T*	8.285	-	-		-	-
2	T1-UL-1Hz	-	0.21	0.30	0.25	2.11	2.47
3	T2-UL-1Hz	-	0.31	0.38	0.21	2.35	3.05
4	T3-UL-1Hz	-	0.43	0.84	0.48	2.99	5.06
5	F1-UL-1Hz – F.D.T	8.28	-	-		-	-
6	T4-UL-1.5Hz	-	0.36	0.42	0.27	1.76	1.39
7	T5-UL-1.5Hz	-	0.51	0.68	0.34	1.63	2.15
8	T6-UL-1.5Hz	-	0.71	0.88	0.25	3.07	3.40
9	F2-UL-1.5Hz – F.D:T	8.21	-	-		-	-
10	T7-UL-6Hz	-	0.14	0.89	0.77	4.18	5.01
11	T8-UL-6Hz	-	0.23	1.77	1.72	12.80	17.05
12	T9-UL-6Hz	-	0.33	1.52	1.76	13.44	18.48
13	F3-UL-6Hz – F.D.T	8.09	-	-		-	-
14	F4-L-1Hz – F.D.T	2.98	-	-		-	-
15	T10-L-1Hz	-	0.22	0.36	0.23	12.33	14.87
16	F5-L-1Hz – F.D:T	2.48	-				
17	T11-L-1Hz FEM correlation	-	0.31	0.53	0.40	22.75	27.78
18	F6-L-1Hz – F.D.T	2.05	-				
19	T12-L-1Hz collapsed	-	0.46 3.54**	1.05 2.17**	0.92	55.03 283.14**	86.04 294.82**

*F.D.T – frequency determination test
** near collapse
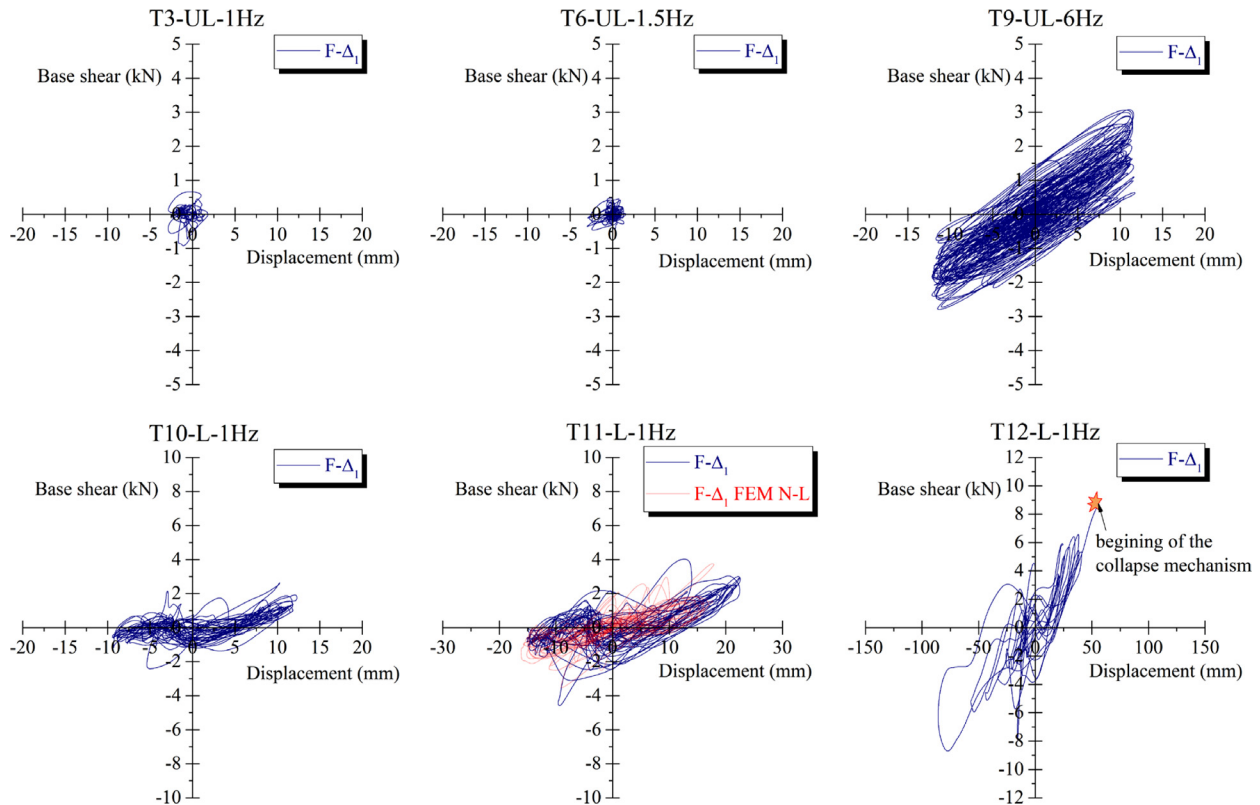
Fig. 16. Base shear vs. displacement graphs.

same time with the onset of plastic deformations of the edges of the pre-drilled holes, mechanism (b). The wall of the clipped steel profile (the chord) is subjected to bending and rotates outwards creating a gap between the chords and the strut during the application of the tensile load, mechanism (d). The excessive rotation is restrained due to the contacts between the chord and the strut. At the same time, the gap the occurs between the steel profiles lowers the friction force and leads to the unscrewing of the STS, mechanism (c).

4.6.2. Bare steel frame model subjected to seismic actions

After the first two series of tests were conducted at frequencies of 1 Hz and 1.5 Hz, no visible deformations could be observed at the joints between the CFS profiles, especially at the ends of the diagonal elements (the most loaded ones). When the frequency of the shaking motion increased to 6 Hz, significant amplifications of the response were recorded in terms of accelerations and relative displacements. The model was inspected once again and no visible damages could be detected for the elements and the joints of the framing in X direction.
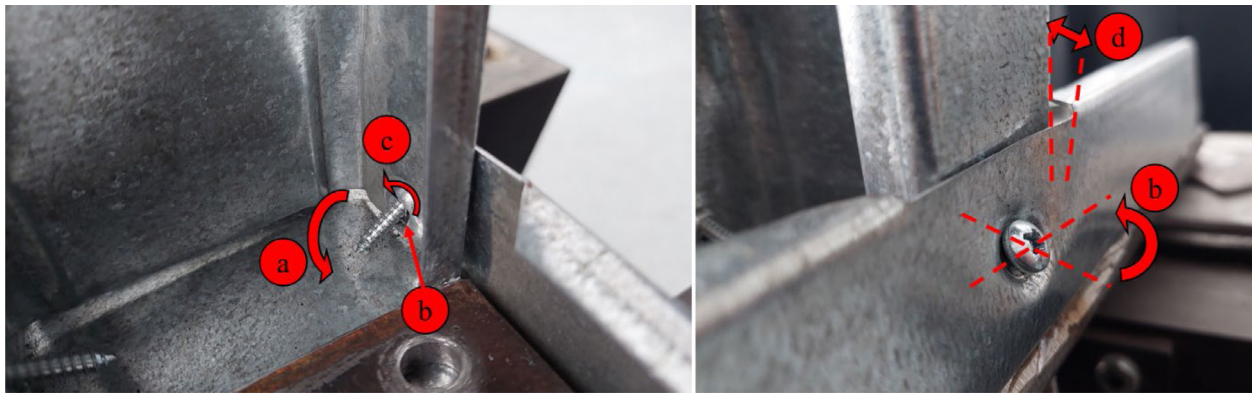
Fig. 17. Failure mechanism in joints during cyclic tests.
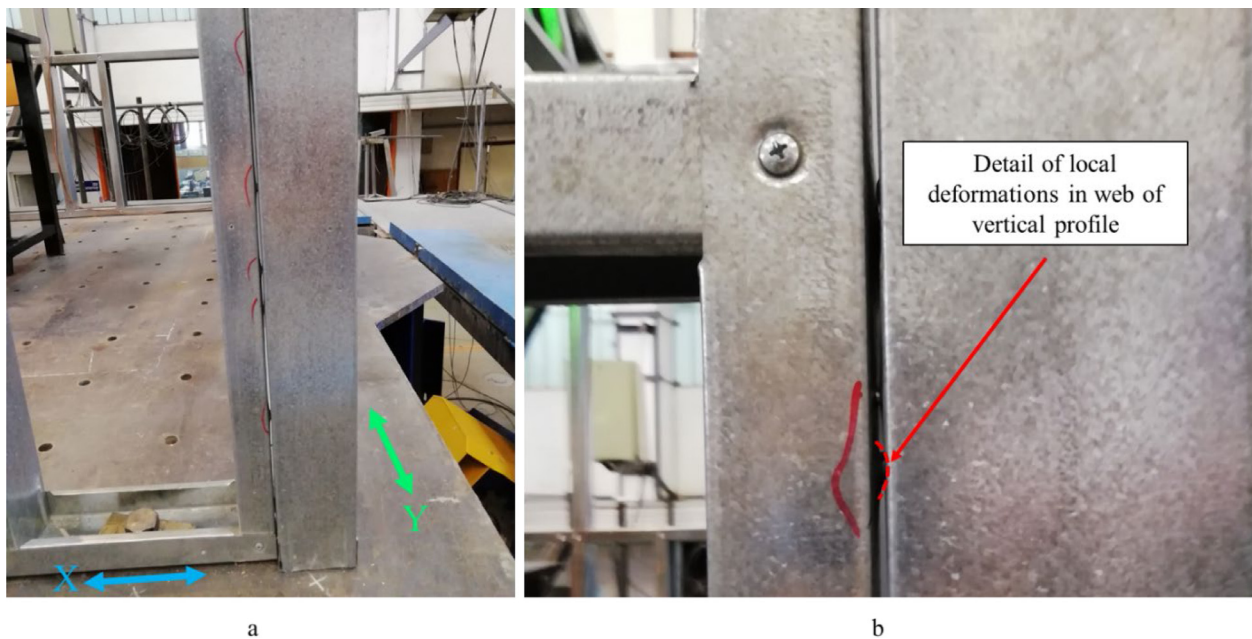
Fig. 18. Deformations of the joints between panels: (a) panel intersection; (b) detail of the deformation.

However, local deformation could be observed at the joints between the framing panels in X and Y directions, as shown in Fig. 18.

During test T11, after the model was loaded with additional masses, the maximum recorded relative displacements was 22 mm. There were still no other visible damages than the ones already identified during the previous tests. During test T12 the model exhibited a relative displacement of 55.03 mm which represented the onset of the failure mechanism, almost at the same time for all 6 locations presented in Fig. 19.

The exact order of the failure mechanisms occurrence in Fig. 19 could not clearly be established because of the extremely short time interval between their occurrences. In case of mechanism **1**, local buckling of the lower chord of the wall framing was observed on both East and West walls (see Fig. 5) which could be caused due to the fixing of the model onto the shake table coupled with the eccentricities between the centerline of the struct and the diagonal element. The axial force it the joint between the diagonal element and the lower chord produced normal stresses that exceeded the yield strength of the material leading to excessive plastic deformations and pulling out of the screw.

Mechanism **2** occurred at the upper end of the diagonal element adjacent to the door gap in the East wall along axis X2 (see Fig. 9). The failures occurred due to the local buckling of the horizontal element

connecting the diagonal element and the vertical one forming the door gap. A similar failure mechanism was identified on the opposite side of the door gap. The 3rd failure mechanisms occurred at the joint between the vertical element and the lower end of the upper diagonal in the East wall. Both the vertical and horizontal elements failed due to local buckling because the joint between the diagonal element and the vertical one was stronger than the other joints due to the presence of an additional screw.

Mechanism **4** occurred in the upper part of the door gap, in the vertical element due to torsional buckling. The presence of the truss system to stiffen the upper part of the door gap led to significant differences in lateral stiffness which may have triggered the failure mechanism 4.

Mechanism **5** occurred due to local buckling of the horizontal element at the top of the door gap in Eastern wall coupled with pulling out of the screw. Mechanism **5** may have influenced the occurrence of mechanism 4 due to the fact that the upper left panel of the door gap lost its in-plane stability.

Mechanism **6** occurred in the Western, at the top end of the lower diagonal element from the panel located between the two windows opening. The failure occurred due to the tearing of the material in the diagonal element.

There were also other local damages identified throughout the model in the form of local crushing of the steel sheet at the edges of

Fig. 19. Failure details mechanisms captured from video recording of the experiment.

the holes of local deformation at the joints between the walls (corners of the model) but without pulling out of the screws.

5. Numerical modeling

5.1. General considerations

The numerical modeling of CFS structures can be accomplished by means of two frequently used approaches aimed at accurately simulating the real behavior of the structure. One of the frequently met approaches in the scientific literature [55–60] consists in using 2D or even 3D elements. Coupled with a non-linear material behavior, this approach leads to very accurate results, but it requires expensive hardware and a lot of time to run the simulations especially in case of complex structures.

On the other hand, the approach presented in the design codes [3, 61,62] suggests that the joints are the most vulnerable components of the CFS structures. The numerical investigations conducted in case of such an approach should take into account the second order effect and the real stiffness of the joints. The latter can be obtained from experimental testing. The numerical models presented in this paper consist in linear and non-linear models with infinitely (1) rigid joints and (2) semi-rigid joints. The rigidity of the latter was considered as constant or having a parabolic variation.

Starting from previously published results [46] and considering the results obtained through cyclic tests on T-joints, the finite element structural model based on 1D-beam pin-connected elements was used to simulate the behavior of the experimental model subjected to a similar loading scenario as in test T11.

5.2. The numerical model

Robot Structural Analysis Professional was used to generate the numerical model [63]. Depending on the type of analysis, linear or non-linear, the joints may be defined by means of their axial stiffness k_x depending on the considered scenario:

1. For the bare frame model:

    a. Linear with joints defined with elastic option $k_x = 5650$ N/mm and simple supports;

    b. Linear with rigid joints defined by $k_x = \infty$ and simple supports;

    c. Nonlinear with $k_x = 5650$ N/mm — parabolic and uplift supports.

2. For the loaded model (additional masses considered):

    a. Linear with joints defined with elastic option $k_x = 5650$ N/mm and simple supports;

    b. Linear with rigid joints defined by $k_x = \infty$ and simple supports;

    c. Nonlinear with $k_x = 2300$ N/mm — parabolic and uplift supports.

Fig. 20a presents the conceptual design/definition of the joint in the local coordinate system of each bar element. Based on the experimentally obtained data from direct tensile tests, Fig. 20b, and cyclic tests, Fig. 20c, the values of the joint stiffness both in tension and compression were assessed as a mean value of 2300 N/mm. The program allows the user to choose from several options on how to define the end releases for each degree of freedom as: fixed (fully restrained, infinite rigidity), fixed values of rigidity or by means of a parabolic variation [63]. Fig. 21 presents the numerical model highlighting the bar ends at the joints.

The geometry of the numerical model was generated based on the exact dimensions of the experimental model, including the eccentricities of the elements at the joints. Rigid joints were considered between the walls. The support conditions were chosen as pin supports at the location of the bolts fixing the model on the shake table. In the case of the non-linear numerical model, FEM N-L, additional uplift support conditions were generated on the surface of the lower chord of the wall framing. Such support conditions have a restrained displacement in the negative direction of the global Z axis (downwards) but the upward displacement was allowed. A graphical representation of the location of supports is presented in Fig. 22. Table 5 summarizes the characteristics of each numerical model considered in the paper.

Newmark method was used for the Time History Analysis (THA) for which the Rayleigh Damping coefficients were computed based on $\omega_1 = 14.72, \xi_1 = 0.02$ and $\omega_2 = 25.54, \xi_2 = 0.02$. The resulting values were $\alpha = 0,3735$ and $\beta = 0,00099$. A 0.02 s time step size was considered which was similar to the time interval for data acquisition during the
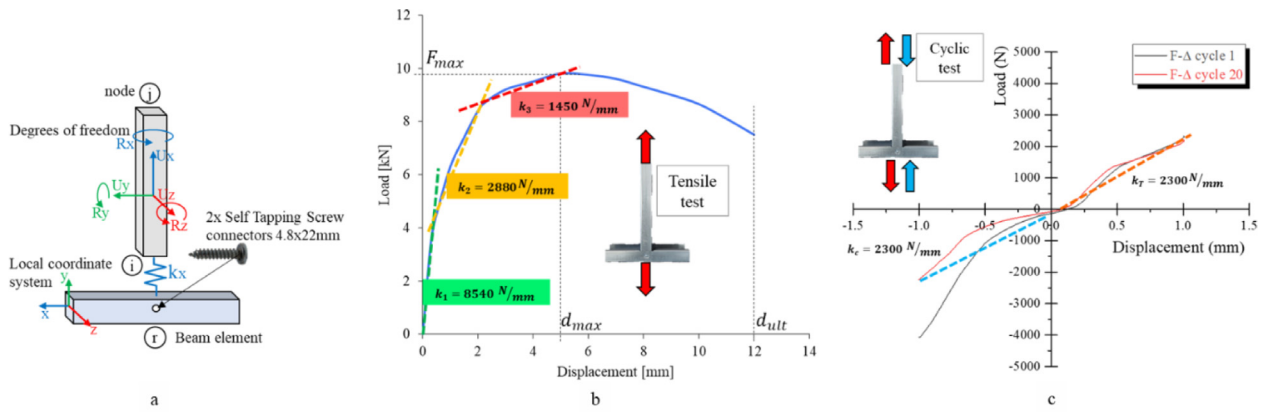
Fig. 20. Definition of beam element end-releases in Robot Structural Analysis (a) joint of beam FEM schematic concept; (b) load–displacement experimental monotonic data test; (c) load–displacement cyclic data test.

Joints definition

Degree of freedom	Beginning	End	Symbol
U_x	Nonlinear joint B	Nonlinear joint B	n
U_y	none	none	x
U_z	none	none	x
R_x	none	none	x
R_y	none	none	x
R_z	released	released	f
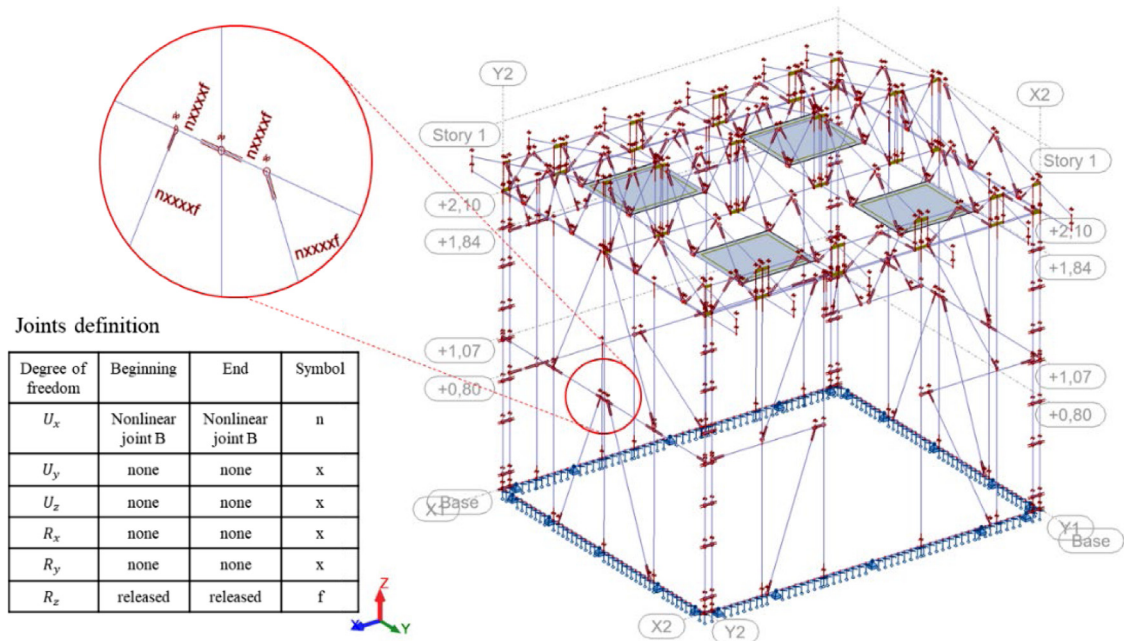
Fig. 21. Numerical model FEM N-L with beam elements and joints definition.
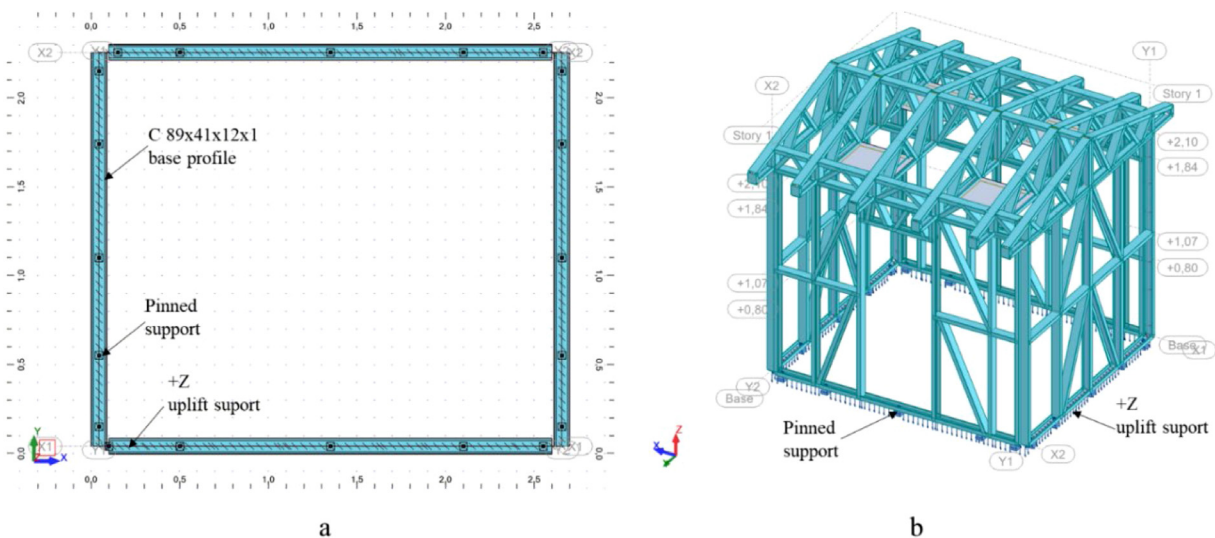
Fig. 22. Numerical model FEM N-L geometry (a) base plan view with supports; (b) 3D spatial model.

Table 5
Numerical models characteristics.

Model analysis type	Number of nodes	Number of bars	Bar finite elements	Rigid links	Releases	Non-linear releases	Supports	Unidirectional supports (uplift +Z)	Static degree of freedom	Time-History analysis method
Linear $k_x = 2300$ N/m	1193	312	897	105	256	–	200		6920	Modal decomposition
Linear $k_x = \infty$	1193	312	897	105	256	–	200		6920	Modal decomposition
Nonlinear $k_x = 2300$ N/mm	1193	312	897	105	–	256	200	181	7101	Newmark method
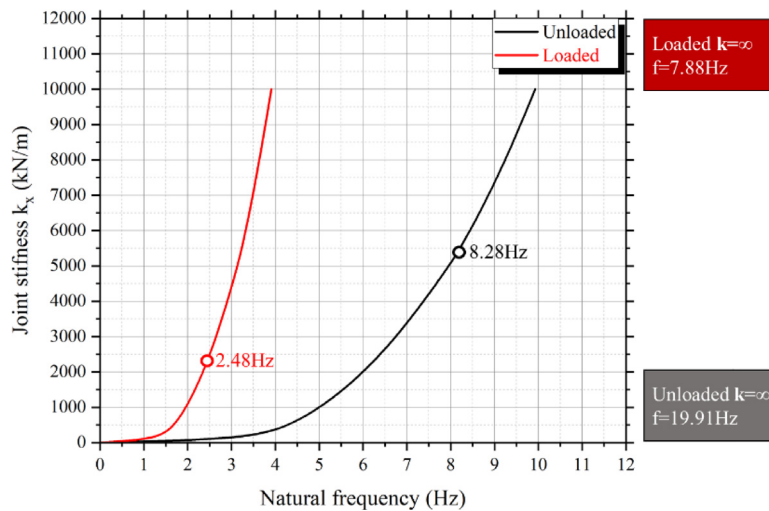
Fig. 23. Joint stiffness vs. natural frequency of the FEM Nonlinear model.

experimental program. The accelerograms used in the numerical model were the ones recorded at the level of the shake table, in both X and Y directions, during test T11-L-1 Hz.

5.3. Dynamic properties of the model

In order to calibrate the model from the point of view of the fundamental frequency of vibration, a set of modal analyses were conducted for which the main parameter was the axial stiffness at the joints. The considered range was between 100 N/mm up to 10000 N/mm. Fig. 23 presents the variation of the fundamental frequency with the change of the axial stiffness at the joints (end of bars). It can be observed that the values of the axial stiffness for which the fundamental frequency of the numerical model matched the experimental data, in both bare/unloaded and loaded frame configurations, were 5650 N/mm and 2300 N/mm, respectively. The axial rigidities exhibited lower values compared to the ones obtained by means of direct tensile tests but similar to the ones obtained during the cyclic tests. For the case of bare/unloaded structure, the considered value of the stiffness should be the one corresponding to the linear elastic range. In case of the loaded structure, already subjected to a three series of seismic motions, the axial rigidity at the joints should be reduced because of the innate displacements that may occur in the joint areas The results obtained from the numerical investigations suggested that the axial rigidity at the joints should be equal to the average value of the secant stiffness obtained from the cyclic tests and presented in Fig. 20c.

Fig. 24 presents the first two mode shapes of the bare/unloaded structural model. It can be observed that both mode shapes are translational ones in X and Y directions, respectively. Fig. 25 presents the first two mode shapes for the loaded structure.

Table 6 summarizes the results obtained from the modal analyses for all considered scenarios. From the presented data it can be observed

that for the numerical model for which the joints were considered to have infinite axial rigidity, the obtained dynamic characteristics of the model differ significantly from the experimental results. It can, therefore, be concluded that this approach would lead to erroneous results.

5.4. Time history analyses

A similar accelerogram to the one corresponding to experimental test T11-L-1 Hz was considered in the numerical model. Both linear and non-linear analyses were run.

Fig. 26 present the response of the model in terms of accelerations and displacements. For comparative purposes, the experimentally obtained results and the numerical ones for different types of THA analyses were plot on the same graph. The output for the numerical model was considered to be at node 65 which corresponds to A_{x1} and D_{x3} on the real model (see Fig. 9).

It can be observed that there are significant differences between the results obtained from each of the two numerical models for which linear analysis was considered. The difference between the two models consisted in the way the axial rigidity was considered at the joints: infinite axial rigidity and finite axial rigidity with a value of 2300 N/mm. At the same time, the numerical model for which a non-linear analysis was considered, lead to similar results as the linear analysis case but with axial rigidity at the nodes defined based on the experimental data. For both graphs presented in Fig. 26, the numerical results are very close to the experimental data during the first 10 s on the THA. After that, the experimental model started to exhibit local damages which could not be captured in the numerical model. For this to happen, non-linear material behavior should also be considered in the numerical simulations which would lead to a more demanding calculation effort.

Fig. 27 presents the deformed shape of the structure in each of the considered scenarios for the THA: (a) nonlinear with $k_x = 2300$ N/mm
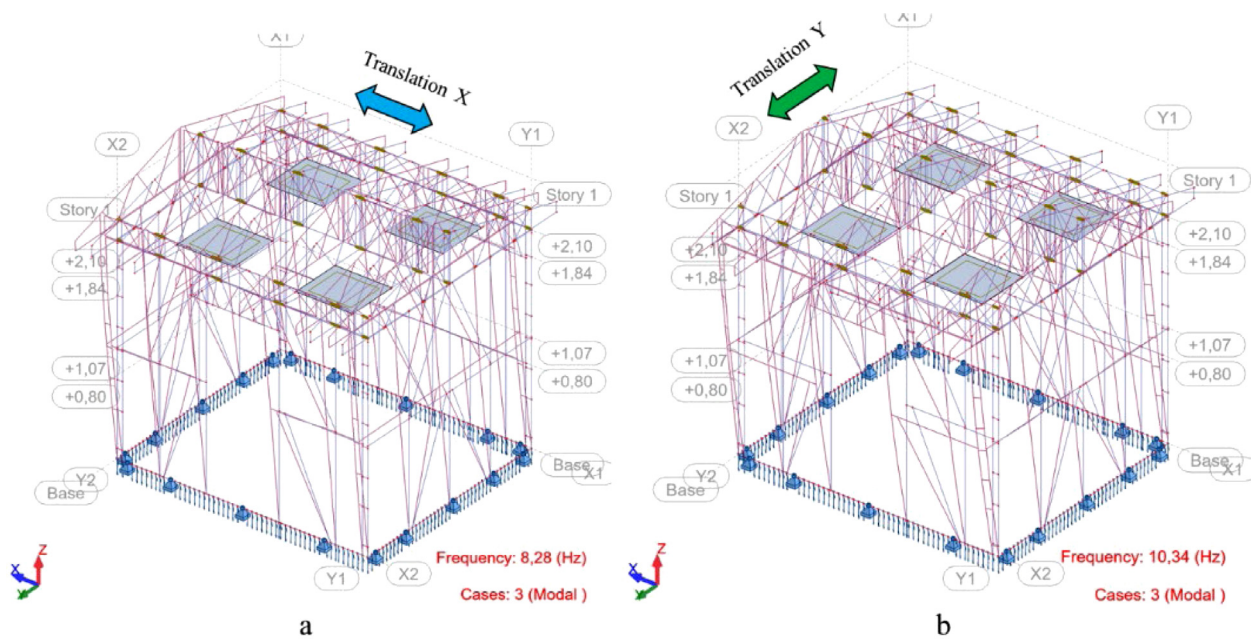
Fig. 24. Vibration modes of nonlinear unloaded-UL model: (a) 1st mode — translation in X direction; (b) 2nd mode — translation in Y direction.
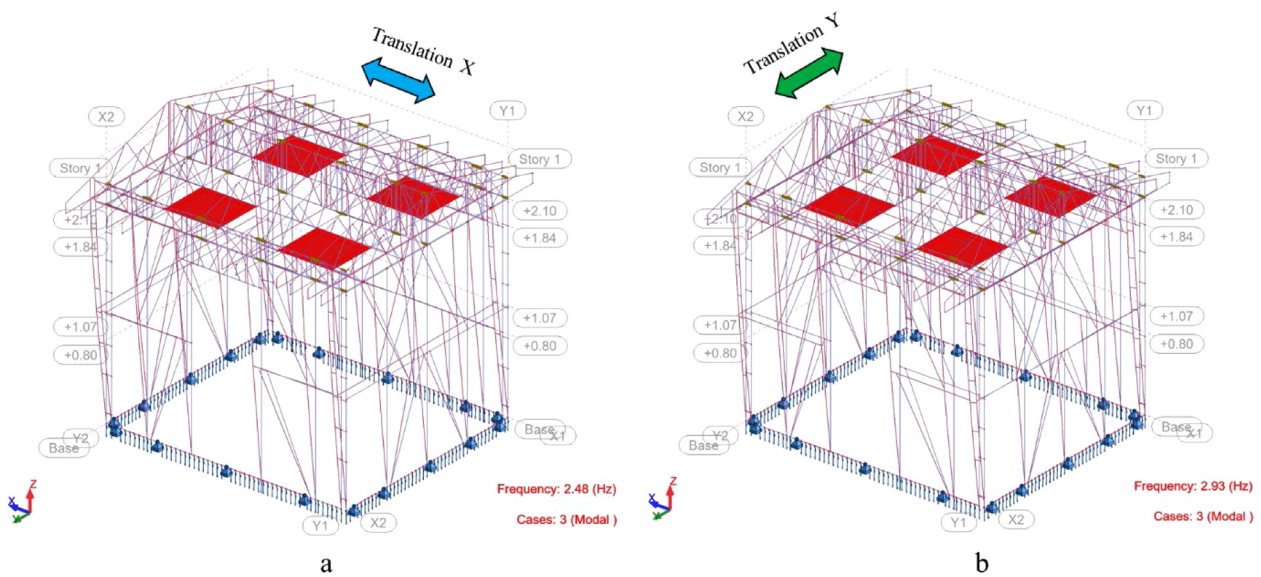
Fig. 25. Vibration modes of nonlinear loaded-L model: (a) 1st mode — translation in X direction; (b) 2nd mode — translation in Y direction.

Table 6
Dynamic analysis results.

Model	Mode	Frequency (Hz)	Period (sec)	Current mass Ux (%)	Current mass Uy (%)	Total mass (kg)	Pulsation	Damping
Unloaded	1	8.28	0.12	83.78	0.01	293	52.05	0.01
FEM k_x = 5650 N/mm	2	10.34	0.10	0.02	84.40	293	64.97	0.01
Unloaded	1	19.93	0.06	85.10	0.01	293	112.04	0.04
FEM k_x=inf	2	26.14	0.05	0.01	84.48	293	125.09	0.04
Unloaded Experimental	1	8.28	0.12	–	–	293	52.05	0.01
Loaded	1	2.48	0.40	96.44	0.05	1496	16.21	0.01
FEM k_x = 2300 N/mm	2	2.73	0.37	0.07	96.66	1496	18.34	0.01
Loaded	1	7.88	0.13	96.89	0	1496	49.54	0.04
FEM k_x = inf	2	10.45	0.10	0	96.78	1496	65.67	0.04
Loaded Experimental	1	2.48	0.40	–	–	1496	15.58	0.02

(b) linear with k_x = 2300 N/mm and (c) linear with k_x = ∞. The maximum intensity of the axial force obtained during the THA for the three considered scenarios is shown in Fig. 28.

It can be observed that the lateral displacements of the linear and nonlinear models with k_x = 2300 N/mm are much larger than in the case of infinite rigidity at the nodes. At the same time, the obtained
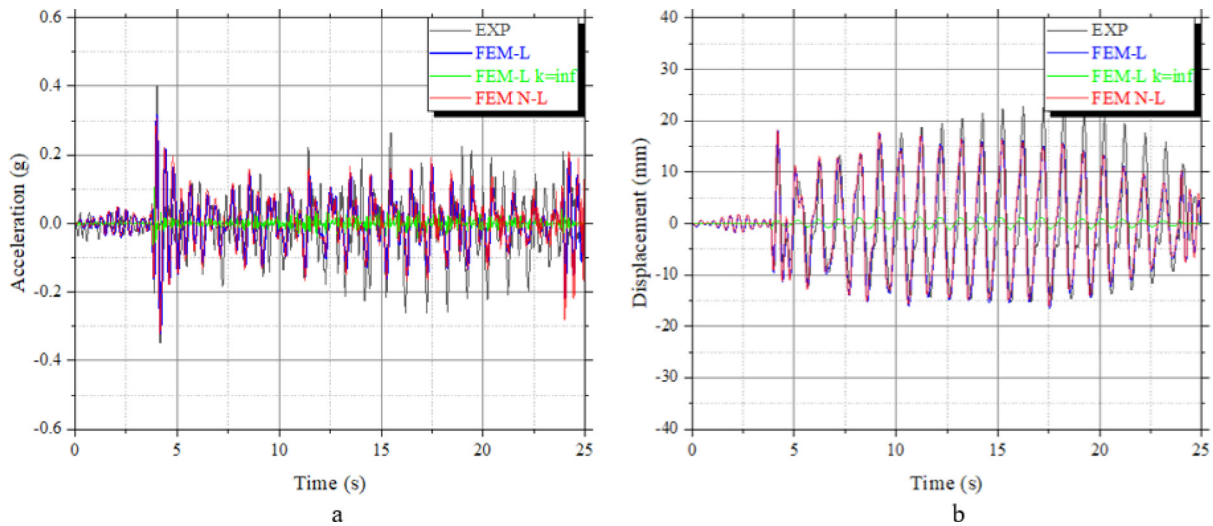
Fig. 26. Results on Loaded-L model, test T11 actions: (a) accelerations; (b) displacements.
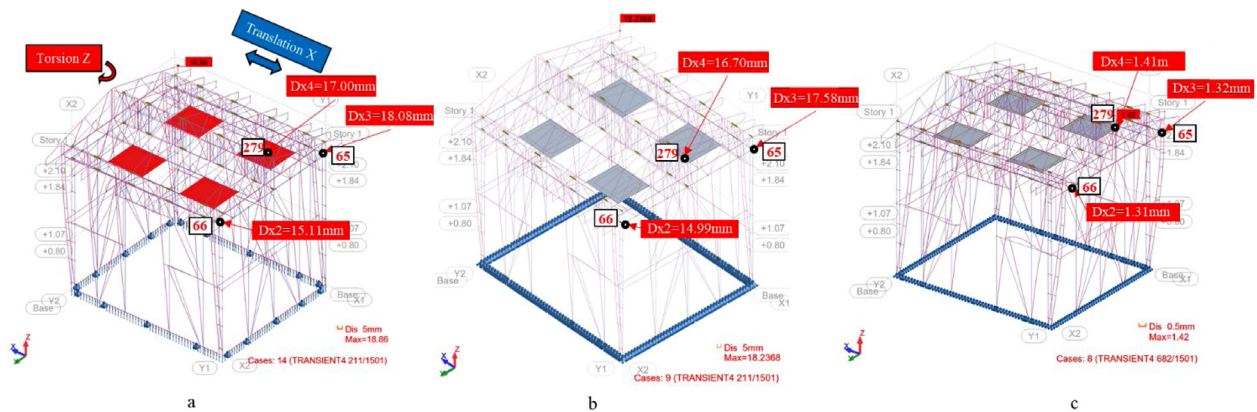
Fig. 27. Time History analysis maximum displacements: (a) Nonlinear model-$k_x = 2300$ N/mm; (b) linear model-$k_x = 2300$ N/mm; (c) linear model $k_x = $ inf.
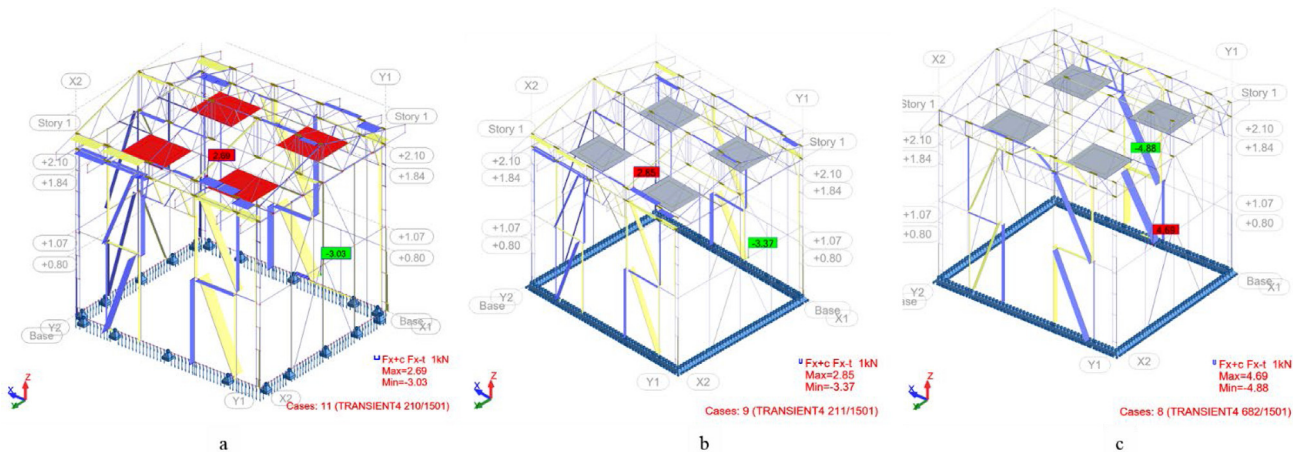
Fig. 28. Maximum axial forces (a) Nonlinear model-$k_x = 2300$ N/mm; (b) linear model-$k_x = 2300$ N/mm; (c) linear model $k_x = $ inf.

values of the lateral displacements at node 66, located at the same level as node 65 but on the opposite wall, are different than the ones obtained at node 65 which suggests that a torsional movement was also present. Considering the geometry of the model and the locations for the door and windows openings, this torsional effect was somehow expected.

The maximum intensity of the axial force, 3.03 kN, occurred in the diagonal element of the lower central panel belonging to West wall where window openings were located. For comparison, in case of the model with infinite axial rigidity at the nodes, the corresponding axial force was 4.69 kN.

6. Discussions

Laboratory cyclic tests conducted on the T-joints showed that they have a lower bearing capacity and a lower stiffness compared to the values obtained from direct tensile tests. Even though on the compression side of the cyclic test the initial tendency of the joint was to behave more rigidly compared to the tensile side, the rigidity in compression was significantly reduced after 20 loading cycles and becomes similar to the one in tension. Similar behavior was observed during the experimental tests on the shake table. The obtained results for the axial rigidity of the joints were used in calibrating the numerical model.

The shaking motions at low frequencies of 1 Hz and 1.5 Hz did not produce significant damages into the structure and resulted in an almost rigid body motion response from the model. Very low values of relative accelerations and displacements were obtained even though the amplitude of the input acceleration was increased up to 0.71 g in case of T6. One possible explanation could be the fact that the frequency of the input motion was far away from the fundamental frequency of vibration of the model, 8.28 Hz. However, based on the determined fundamental frequency after each series of tests, it resulted those slight damages could be present in the model since the fundamental frequency decreased to 8.21 Hz, a 0.8% decrease. This small difference may also be due to the inherent measurement errors.

When the frequency of the input motion increased to 6 Hz, larger lateral displacements could be observed. However, the model was still in the linear elastic range of material behavior and the decrease in the fundamental frequency of vibration to 8.09 Hz after the third series of tests could be attributed to the small displacements starting to occur at the joints. This would lead to a more flexible model. The maximum relative displacements increased to 13.44 mm and the relative acceleration reached 1.76 g. The large amplification of the shaking motion, especially in terms of accelerations, could be explained by the ratio of 0.8 between the frequency of the input motion and the fundamental frequency of the model.

The model was loaded with additional masses which would amount to an equivalent load of 1.80 kN/m². The increased weight resulted in a 63% decrease in the value of the fundamental frequency from 8.09 Hz to 2.98 Hz. For the loaded model, only a sine beat input motion with a frequency of 1 Hz was selected but with different amplitudes of the input signal. It was observed that during test T11 the relative displacement increased to 22 mm which exceeded the maximum values for ULS by 100%. The fundamental frequency of the model decreased by 16.8% to 2.48 Hz.

During the test T12 the response of the structure was significantly amplified due to damages in the elements and joints and possible resonance phenomenon on higher modes of vibration. After 20 s the relative displacement exceeded 86 mm and failure mechanisms started to develop. This led to further amplification in the response of the structure due to the fact that the fundamental frequency of the model dropped below 2 Hz and became very close to the frequency of the input motion.

The experimental program revealed a complex failure mechanism which can be considered as:

- Global Rocking — a slight uplift of the lower chords of the framing walls between the connection points between the model and the shake table;
- Local buckling of compressed elements such as diagonal elements and even vertical ones near the joints;
- Local buckling of horizontal elements;
- Plastic deformations at the edges of the pre-drilled holes in the CFS profiles;
- Tilting and pulling out of the screws at the joints;
- Tearing of elements in the joint area corresponding to the net cross-sectional area of CFS profile.

- Unfasten of screws at the joints.
- The overall stiffness of the whole structure during the tests decreased due to damages located in general in connections between structural elements. The level of energy absorption is low.

The information collected during the experimental program serves as the starting point for a new series of experiments on similar models with different cladding options such as OSB or gypsum boards. They also served as calibration data for the numerical model developed within the framework of the present research.

The numerical investigation included both linear and non-linear analyses with finite values of axial stiffness at the end of the bar elements determined from cyclic tests. It was observed that for a value of the axial stiffness of 2300 N/mm the results obtained by means of FEA matched the experimental ones very well. Moreover, the values of the relative displacements and accelerations were very close to the ones obtained during the shake table tests. However, the fact that the numerical model did not consider any material non-linearities, only geometrical ones, resulted in quite large differences between the obtained results especially after the experimental model started to exhibit damages due to repeated shaking motions.

7. Conclusions

The paper presents the results obtained after a complex experimental program coupled with numerical simulations on a scaled-down model, 1/1.2 scale, of a CFS structure made of 89 × 41×12× x1 mm lipped channel elements. It represents a replica of constructive solutions for ground floor or ground floor and one or two storeys structures that are frequently met in South-East Europe, including highly active seismic areas.

The main purpose of the research program is to gather both quantitative but more importantly, accurate information in terms of structural response to dynamic actions characterized by input accelerations equal in amplitude to the maximum values specified in seismic design codes, PGA=0.40 g. Comparing both experimental and numerical results obtained for the relative displacements with the maximum allowed values specified in the code for ULS (0.005H) and SLS (0.025H) it can be concluded that the overall stiffness of the structure is able to fulfill the imposed conditions. It was observed that the small values of damping from 0.01 to 0.02 for such structural systems without cladding materials, means they have low energy dissipation capabilities.

The damage of the joints and the reduction in the structural stiffness due to cyclic loads, such as the ones produced by earthquakes, change the eigen period of the structure and has a significant influence on the response of the structure to seismic actions. Larger gravitational loads lead to more extensive damage to the joints.

The developed numerical model based on the experimentally determined connection axial rigidity is able to offer accurate results in terms of the fundamental frequency of vibration, relative accelerations and displacements. This accuracy can be obtained even by running simple linear static and THA analyses, without the need for complex and computationally intensive non-linear approaches. However, for a more accurate capturing of the local damages and onset of failure mechanisms, more complex numerical models are needed, which take into account non-linear material behavior.

The results presented in this paper serve as a starting point for future research works aimed at assessing the influence of the sheathing on the response of CFS structures to seismic actions. Additionally, research in the direction of improved joints with better energy dissipation properties is also pursued by the authors.

CRediT authorship contribution statement

George Taranu: Writing – original draft, Software, Project administration, Methodology, Investigation, Funding acquisition, Data curation, Conceptualization. **Viorel Ungureanu:** Writing – review & editing, Validation, Supervision, Conceptualization, Investigation, Writing – original draft. **Zsolt Nagy:** Writing – review & editing, Validation, Supervision, Investigation, Writing – original draft. **Mihai-Sergiu Alexa-Stratulat:** Methodology, Data curation. **Ionut-Ovidiu Toma:** Writing – original draft, Investigation, Methodology, Writing – review & editing. **Septimiu-George Luca:** Software, Formal analysis, Data curation.

Declaration of competing interest

The authors declare that they have no known competing financial interests or personal relationships that could have appeared to influence the work reported in this paper.

Data availability

Data will be made available on request.

Additional information

Video shaking table experiment: https://youtu.be/IcGuz9mW8l4
Video Time History vs. Experiment: https://youtu.be/tZVaSpgGxy4
Video of direct tensile tests on T-joints: https://youtu.be/v0yRbs4f WvM
Video of cyclic tests on T-joints: https://youtu.be/eujWg-R-O2U

References

[1] EN 1998-1, Eurocode 8: Design of Structures for Earthquake Resistance – Part 1: General Rules, Seismic Actions and Rules for Buildings, CEN, Brussels, Belgium, 2004.

[2] P100/2013-1, Seismic Design Code - Part I: Design Rules for Buildings, M.D.L.P.A Romania, 2013, (in Romanian).

[3] EN 1993-1-3, Eurocode 3: Design of Steel Structures, Part 1.3: General Rules, Supplementary Rules for Cold-Formed Thin Gauge Members and Sheeting, CEN, Brussels, Belgium, 2006.

[4] EN 1993-1-5, Eurocode 3: Design of Steel Structures-Part 1-5: Plated Structural Elements, CEN, Brussels, Belgium, 2006.

[5] S.K. Naman, B.J. Goodno, Seismic evaluation of a low rise steel building, Eng. Struct. 8 (1986) 9–16, http://dx.doi.org/10.1016/0141-0296(86)90014-3.

[6] R.T. Severn, D.P. Stoten, Y. Tagawa, The contribution of shaking tables to earthquake engineering, in: 15 WCEE, 2012.

[7] B.W. Schafer, D. Ayhan, J. Leng, P. Liu, D. Padilla-Llano, K.D. Peterman, M. Stehman, S.G. Buonopane, M. Eatherton, R. Madsen, B. Manley, C.D. Moen, N. Nakata, C. Rogers, C. Yu, Seismic response and engineering of cold-formed steel framed buildings, Structures 8 (2016) 197–212, http://dx.doi.org/10.1016/j.istruc.2016.05.009.

[8] K.D. Peterman, M.J.J. Stehman, R.L. Madsen, S.G. Buonopane, N. Nakata, B.W. Schafer, Experimental seismic response of a full-scale cold-formed steel-framed building. I: System-level response, J. Struct. Eng. 142 (2016) http://dx.doi.org/10.1061/(asce)st.1943-541x.0001577.

[9] B.W. Schafer, Cold-formed steel structures around the world, Steel Constr. 4 (2011) 141–149, http://dx.doi.org/10.1002/STCO.201110019.

[10] N. Nakata, B.W. Schafer, R.L. Madsen, Seismic design of multi-story cold-formed steel buildings: The CFS-NEES archetype building, in: Structures Congress 2012 - Proceedings of the 2012 Structures Congress, 2012, http://dx.doi.org/10.1061/9780784412367.134.

[11] K.D. Peterman, R.L. Madsen, B.W. Schafer, Experimental seismic behavior of the CFS-NEES building: System- level performance of a full-scale two-story light steel framed building, in: 22nd International Specialty Conference on Recent Research and Developments in Cold-Formed Steel Design and Construction, 2014.

[12] P. Liu, K.D. Peterman, C. Yu, B.W. Schafer, Cold-formed steel shear walls in ledger-framed buildings, in: Structural Stability Research Council Annual Stability Conference, 2012.

[13] X. Wang, T.C. Hutchinson, Evolution of modal characteristics of a mid-rise cold-formed steel building during construction and earthquake testing, Int. J. Earthq. Eng. Struct. Dyn. 49 (2020) 1539–1558, http://dx.doi.org/10.1002/EQE.3316.

[14] R. Landolfo, O. Iuorio, L. Fiorino, Experimental seismic performance evaluation of modular lightweight steel buildings within the ELISSA project, Earthq. Eng. Struct. Dyn. 47 (2018) http://dx.doi.org/10.1002/eqe.3114.

[15] V. Macillo, L. Fiorino, R. Landolfo, Seismic response of CFS shear walls sheathed with nailed gypsum panels: Experimental tests, Thin-Walled Struct. 120 (2017) 161–171, http://dx.doi.org/10.1016/j.tws.2017.08.022.

[16] L. Fiorino, V. Macillo, R. Landolfo, Shake table tests of a full-scale two-story sheathing-braced cold-formed steel building, Eng. Struct. 151 (2017) 633–647, http://dx.doi.org/10.1016/j.engstruct.2017.08.056.

[17] R. Landolfo, A. Campiche, O. Iuorio, L. Fiorino, Seismic performance evaluation of CFS strap-braced buildings through experimental tests, Structures 33 (2021) http://dx.doi.org/10.1016/j.istruc.2021.05.098.

[18] S. Shakeel, B. Bucciero, A. Campiche, T. Pali, L. Fiorino, R. Landolfo, Shake table testing and numerical modelling of LWS strap-braced structures for seismic performance evaluation, in: AIP Conference Proceedings, 2019, http://dx.doi.org/10.1063/1.5114270.

[19] A. Campiche, S. Shakeel, B. Bucciero, T. Pali, L. Fiorino, R. Landolfo, Seismic behaviour of strap-braced LWS structures: Shake table testing and numerical modelling, in: IOP Conference Series: Materials Science and Engineering, 2019, http://dx.doi.org/10.1088/1757-899X/473/1/012032.

[20] M.T. Terracciano, B. Bucciero, T. Pali, V. Macillo, L. Fiorino, R. Landolfo, Shake table tests of structures with CFS strap-braced stud walls, Key Eng. Mater. 763 (2018) http://dx.doi.org/10.4028/www.scientific.net/KEM.763.432.

[21] V. Macillo, A. Campiche, S. Shakeel, B. Bucciero, T. Pali, M.T. Terracciano, L. Fiorino, R. Landolfo, Seismic behaviour of sheathed CFS buildings: Shake-Table testing and numerical modelling, Key Eng. Mater. 763 (2018) http://dx.doi.org/10.4028/www.scientific.net/KEM.763.584.

[22] A. Campiche, S. Shakeel, V. Macillo, M.T. Terracciano, B. Bucciero, T. Pali, L. Fiorino, R. Landolfo, Seismic behaviour of sheathed CFS buildings: Shake table tests and numerical modelling, Ingen. Sismica 35 (2018).

[23] D. Dubina, Behavior and performance of cold-formed steel-framed houses under seismic action, J. Construct. Steel Res. 64 (2008) 896–913, http://dx.doi.org/10.1016/J.JCSR.2008.01.029.

[24] L.A. Fülöp, D. Dubina, Performance of wall-stud cold-formed shear panels under monotonic and cyclic loading: Part II: Numerical modelling and performance analysis, Thin-Walled Struct. 42 (2004) 339–349, http://dx.doi.org/10.1016/S0263-8231(03)00064-8.

[25] D. Dubina, L. Fülöp, V. Ungureanu, I. Szabo, Z. Nagy, Cold-Formed Steel Structures for Residential and Non-Residential Buildings, Timisoara, 2000.

[26] D. Dubina, L.A. Fülöp, A. Aldea, S. Demetriu, Z. Nagy, Seismic performance of cold-formed steel framed houses, in: Proceedings of 5th International Conf. on Behaviour of Steel Structures in Seismic Areas (STESSA), Yo1kohama, 2006, pp. 429–435.

[27] D. Dubina, A. Stratan, A. Ciutina, L. Fulop, Z. Nagy, Strength, stiffness and ductility of cold-formed steel bolted connections, in: International Workshop on Connections in Steel Structures V, Behaviour, Strength & Design, 2004.

[28] V. Ungureanu, I. Both, M. Burca, B. Radu, C. Neagu, D. Dubina, Experimental and numerical investigations on built-up cold-formed steel beams using resistance spot welding, Thin–Walled Struct. 161 (2021) http://dx.doi.org/10.1016/j.tws.2021.107456.

[29] O. Senkardesler, G. Goler, S. Soyoz, Dynamic and cyclic response of a full-scale 2-storey cold-formed steel structure with and without infill materials, Bull. Earthq. Eng. 15 (2017) 3207–3226, http://dx.doi.org/10.1007/s10518-016-0042-1.

[30] C. Hui, L. Gardner, D.A. Nethercot, Moment redistribution in cold-formed steel continuous beams, Thin-Walled Struct. 98 (2016) 465–477, http://dx.doi.org/10.1016/J.TWS.2015.10.009.

[31] P. Kyvelou, L. Gardner, D.A. Nethercot, Composite Action Between Cold-Formed Steel Beams and Wood-Based Floorboards, vol. 15, 2015, http://dx.doi.org/10.1142/S0219455415400295.

[32] J. Wang, W. Wang, Y. Xiao, B. Yu, Cyclic test and numerical analytical assessment of cold-formed thin-walled steel shear walls using tube truss, Thin-Walled Struct. 134 (2019) 442–459, http://dx.doi.org/10.1016/J.TWS.2018.09.038.

[33] X. Wang, T.C. Hutchinson, G. Hegemier, Seismic behavior of cold-formed steel shear walls during full-scale building shake table tests, in: Wei-Wen Yu International Specialty Conference on Cold-Formed Steel Structures 2018 - Recent Research and Developments in Cold-Formed Steel Design and Construction, 2018.

[34] C. Wang, Z. Yang, Z. Zhang, R. Qi, Experimental study on shear behavior of cold-formed steel shear walls with bracket, Structures 32 (2021) 448–460, http://dx.doi.org/10.1016/j.istruc.2021.03.064.

[35] Y. Zou, X. Zhou, Y. Shi, Z. Wang, K. Ke, Z. Zhang, Y. Guan, Shear resistance of cold-formed thin-walled steel inter-story connections, J. Construct. Steel Res. 183 (2021) http://dx.doi.org/10.1016/j.jcsr.2021.106757.

[36] A. Singh, X. Wang, S. Torabian, T.C. Hutchinson, K.D. Peterman, B.W. Schafer, Seismic performance of symmetric unfinished CFS in-line wall systems, in: Structures Congress 2020 - Selected Papers from the Structures Congress 2020, 2020, http://dx.doi.org/10.1061/9780784482896.058.

[37] H.J. Kim, D.H. Shin, Shake table test program of cold-formed steel in-plane partition walls, Structures 30 (2021) http://dx.doi.org/10.1016/j.istruc.2021.01.026.

[38] Y. Guan, X. Zhou, X. Yao, Y. Shi, Seismic performance of prefabricated sheathed cold-formed thin-walled steel buildings: Shake table test and numerical analyses, J. Construct. Steel Res. 167 (2020) http://dx.doi.org/10.1016/j.jcsr.2019.105837.

[39] J. Jing, G.C. Clifton, K. Roy, J.B.P. Lim, Three-storey modular steel building with a novel slider device: Shake table tests on a scaled down model and numerical investigation, Thin-Walled Struct. 155 (2020) 106932, http://dx.doi.org/10.1016/J.TWS.2020.106932.

[40] L. Jiang, K. Yu, J. Ye, Y. Hu, L. Jiang, Seismic damage assessment and shaking-table test validation of midrise cold-formed steel composite shear wall buildings, J. Struct. Eng. 148 (2022) 04022093, http://dx.doi.org/10.1061/(ASCE)ST.1943-541X.0003387.

[41] Y. Hu, L. Jiang, J. Ye, X. Zhang, L. Jiang, Seismic responses and damage assessment of a mid-rise cold-formed steel building under far-fault and near-fault ground motions, Thin-Walled Struct. 163 (2021) 107690, http://dx.doi.org/10.1016/J.TWS.2021.107690.

[42] L. Jiang, J. Ye, Redundancy of a mid-rise CFS composite shear wall building based on seismic response sensitivity analysis, Eng. Struct. 200 (2019) 109647, http://dx.doi.org/10.1016/J.ENGSTRUCT.2019.109647.

[43] L. Jiang, J. Ye, Quantifying the effects of various uncertainties on seismic risk assessment of CFS structures, 18, 2020, pp. 241–272, http://dx.doi.org/10.1007/s10518-019-00726-w.

[44] I.-O. Toma, M. Budescu, G. Albu, Seismic behaviour of an experimental model made of thin-walled cold formed steel profiles - Hardell structures, in: The Bulletin of the Polytechnic Institute of Jassy, Construction. Architecture Section, vol. 67, 2009.

[45] A. Firouzianhaij, N. Usefi, B. Samali, P. Mehrabi, Shake table testing of standard cold-formed steel storage rack, Appl. Sci. 2021 (2021) 1821, http://dx.doi.org/10.3390/app11041821.

[46] G. Taranu, I.O. Toma, Experimental investigation and numerical simulation of c-shape thin-walled steel profile joints, Buildings 11 (2021) http://dx.doi.org/10.3390/buildings11120636.

[47] TR Group, Self Drilling Screw, DIN 7504N ~ISO 15481. (n.d.). https://www.trfastenings.com/Products/Catalogue/Screws-and-Bolts/Self-Drilling-Screws/Pan-Head/Cross-Recess-H-Drive (accessed May 4, 2022).

[48] TR Group, Screws Mechanical Properties ISO 898-1 EN 20898-1, (n.d.). https://www.trfastenings.com/products/knowledgebase/steel-fasteners/screws-and-bolts-mechanical-properties (accessed May 4, 2022).

[49] TR Group, Self Tapping Screw, DIN 7981C ~ISO 7049. (n.d.). https://www.trfastenings.com/Products/Catalogue/Screws-and-Bolts/Self-Tapping-Screws/Pan-Head/Cross-Recess-H-Drive/Form-C (accessed May 4, 2022).

[50] P.D. Moncarz, Helmut Krawinkler, Theory and Application of Experimental Model Analysis in Earthquake Engineering, Stanford, California, 1981.

[51] P. Candeias, A. Campos Costa, E. Coelho, Shaking TableTests of 1:3 Reduced Scale Models of Four Story Unreinforced Masonry Buildings, in: 3 Th World Conference on Earthquake Engineering S, 2004.

[52] Mapping Europe's earthquake risk | Research and Innovation, (n.d.), https://ec.europa.eu/research-and-innovation/en/horizon-magazine/mapping-europes-earthquake-risk (accessed April 1, 2022).

[53] ISO 12106:2017(E) - Metallic materials-fatigue testing - Axial-strain-controlled method, 2017.

[54] ASTM E606/E606M-12 - Standard Test Method for Strain-Controlled Fatigue Testing, 2012, http://dx.doi.org/10.1520/E0606-04E01.

[55] M. Kotełko, J. Grudziecki, V. Ungureanu, D. Dubina, Ultimate and post-ultimate behaviour of thin-walled cold-formed steel open-section members under eccentric compression. Part I: Collapse mechanisms database (theoretical study), Thin-Walled Struct. 169 (2021) 108366, http://dx.doi.org/10.1016/J.TWS.2021.108366.

[56] Ł. Borkowski, J. Grudziecki, M. Kotełko, V. Ungureanu, D. Dubina, Ultimate and post-ultimate behaviour of thin-walled cold-formed steel open-section members under eccentric compression. Part II: Experimental study, Thin-Walled Struct. 171 (2022) 108802, http://dx.doi.org/10.1016/J.TWS.2021.108802.

[57] N. Usefi, P. Sharafi, H. Ronagh, Numerical behaviour analysis of cold-formed steel framed walls: State of the art, evaluation and challenges, Thin-Walled Struct. 138 (2019) 252–285, http://dx.doi.org/10.1016/J.TWS.2019.02.019.

[58] I. Shamim, C.A. Rogers, Numerical modelling and calibration of CFS framed shear walls under dynamic loading, in: 21st International Specialty Conference on Cold-Formed Steel Structures - Recent Research and Developments in Cold-Formed Steel Design and Construction, 2012.

[59] A.A. Kasimzade, S. Tuhta, G. Atmaca, S. Ozdemir, Analytical and experimental modal analysis of a model cold formed steel (CFS) structures using microtremor excitation, in: Seismic Isolation, Structural Health Monitoring, and Performance Based Seismic Design in Earthquake Engineering: Recent Developments, 2018, http://dx.doi.org/10.1007/978-3-319-93157-9_9.

[60] A. Campiche, L. Fiorino, R. Landolfo, Numerical modelling of CFS two-storey sheathing-braced building under shaking-table excitations, J. Construct. Steel Res. 170 (2020) http://dx.doi.org/10.1016/j.jcsr.2020.106110.

[61] EN 1993-1-8, Eurocode 3: Design of steel structures - Part 1-8: Design of joints, CEN, Brussels, Belgium, 2005.

[62] EN 1993-1-1, Eurocode 3: Design of Steel Structures - Part 1-1: General Rules and Rules for Buildings, CEN, Brussels, Belgium, 2005.

[63] Robot Structural Analysis Professional, (n.d.). https://www.autodesk.com/products/robot-structural-analysis/overview (accessed January 13, 2022).